

## 1 Comprehensive Dynamics in a Polyelectrolyte Complex Coacervate

2 Khalil Akkaoui, Zachary A. Digby, Changwoo Do, and Joseph B. Schlenoff\*

Cite This: <https://doi.org/10.1021/acs.macromol.3c01540>

Read Online

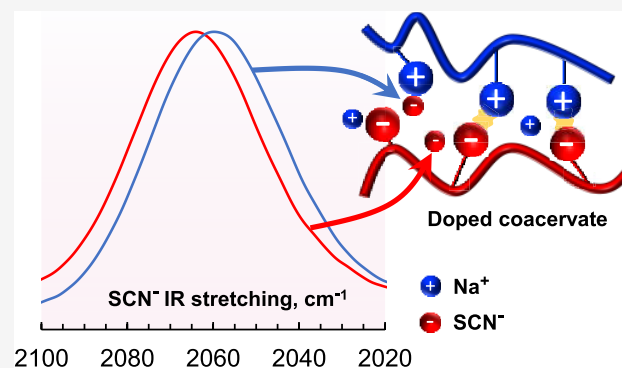
ACCESS |

Metrics &amp; More

Article Recommendations

Supporting Information

3 **ABSTRACT:** The linear viscoelastic response, LVR, of a hydrated  
 4 polyelectrolyte complex coacervate, PEC, was evaluated over a range  
 5 of frequencies, temperatures, and salt concentrations. The PEC was a  
 6 nearly stoichiometric blend of a quaternary ammonium poly([3-  
 7 (methacrylamido)propyl]trimethylammonium chloride), PMAP-  
 8 TAC, and poly(2-acrylamido-2-methyl-1-propanesulfonic acid so-  
 9 dium salt), PAMPS, an aliphatic sulfonate, selected because they  
 10 remain fully charged over the conditions of use. Narrow molecular  
 11 weight distribution polyelectrolytes were prepared using fractiona-  
 12 tion techniques. A partially deuterated version of PMAPTAC was  
 13 incorporated to determine the coil radius of gyration,  $R_g$ , within  
 14 PECs using small-angle neutron scattering. Chain dimensions were  
 15 determined to be Gaussian with a Kuhn length of 2.37 nm, which  
 16 remained constant from 25 to 65 °C. The LVR for a series of matched molecular weight PECs, mostly above the entanglement  
 17 threshold, exhibited crossovers of modulus versus frequency classically attributed to the reptation time, relaxation between  
 18 entanglements, and the relaxation of a Kuhn length of units (the “monomer” time). The scaling for zero shear viscosity,  $\eta_0$ , versus  
 19 chain length,  $N$ , was  $\eta_0 \sim N^{3.1}$ , in agreement with “sticky reptation” theory. The lifetime and activation energy,  $E_p$ , of a pair between  
 20 polyanion and polycation repeat units,  $\text{Pol}^+\text{Pol}^-$ , were determined from diffusion coefficients of salt ions within the PEC. The  
 21 activation energy for LVR of salt-free PECs was  $2E_p$ , showing that the key mechanism limiting the dynamics of undoped PECs is pair  
 22 exchange. An FTIR technique was used to distinguish whether  $\text{SCN}^-$  acts as a counterion or a co-ion within PECs. Doping of PECs  
 23 with NaSCN breaks  $\text{Pol}^+\text{Pol}^-$  pairing efficiently, which decreases effective cross-linking and decreases viscosity. An equation was  
 24 derived that quantitatively predicts this effect.



## 25 ■ INTRODUCTION

26 An intriguing soft material spontaneously phase separates when  
 27 solutions of polyelectrolytes with opposite charges are mixed.  
 28 When immersed in aqueous solutions, these polyelectrolyte  
 29 complexes retain substantial amounts of water, yet they display  
 30 properties ranging from glassy (below a well-defined glass  
 31 transition temperature,  $T_g$ ), to rubbery/liquidlike above  $T_g$ .<sup>1</sup>  
 32 Complexes above their  $T_g$  at room temperature are usually  
 33 termed “coacervates,” a definition originating from the droplet-  
 34 like morphologies of biopolymer complexes observed by  
 35 Bungenberg de Jong and co-workers.<sup>2</sup> Here, the term PEC is  
 36 used in its most general sense to mean polyelectrolyte  
 37 complexes or coacervates.

38 Microscopic representations of PECs usually depict pairing  
 39 of repeat units on the polycation,  $\text{Pol}^+$ , and polyanion,  $\text{Pol}^-$ ,  
 40 illustrated in Scheme 1, which shows a stoichiometric PEC  
 41 with equal numbers of positive and negative repeat units.  
 42  $\text{Pol}^+\text{Pol}^-$  charge pairs that have appreciable lifetimes can be  
 43 considered to be physical cross-links.

44 The cross-link is a fundamental construct in macromolecular  
 45 science. If permanent, cross-links make glassy materials stiffer,  
 46 or they turn liquid-like polymers into rubbery ones.<sup>3</sup> There has  
 47 been intense interest in dynamic cross-links, which may be

chemical or physical in nature.<sup>4,5</sup> The latter category includes 48  
 hydrogen bonding<sup>6</sup> and “electrostatic” interactions such as 49  
 those represented in Scheme 1. 50

The addition of salt,  $\text{M}^+\text{A}^-$ , introduces a processing 51  
 dimension not available to neutral polymers: as more salt is 52  
 added to solution, it enters the PEC and breaks interactions 53  
 between polymers.<sup>7</sup> This effective decrease in cross-link 54  
 density makes the PEC more fluidlike. Added salt transforms 55  
 a glassy polymer into a rubbery one, enabling processing such 56  
 as extrusion,<sup>8</sup> spin coating,<sup>9</sup> bar coating,<sup>10</sup> embossing,<sup>11</sup> 57  
 compression,<sup>7,12</sup> and electrospinning.<sup>13</sup> This “saloplasticity” 58  
 promotes self-healing driven by enhanced chain mobility at 59  
 intermediate salt concentrations.<sup>7</sup> 60

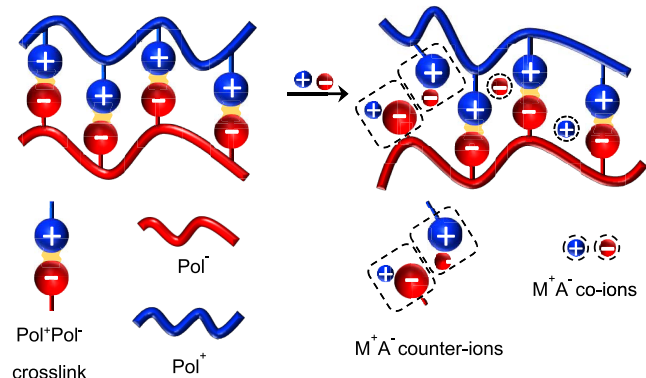
Salt effects on polyelectrolyte solution conformations and 61  
 properties are usually explained using continuum electrostatics 62  
 arguments, wherein salt “shields” Coulombic interactions 63

Received: August 2, 2023

Revised: October 11, 2023

Accepted: January 4, 2024

**Scheme 1. Depiction of a Stoichiometric PEC Showing Pol<sup>+</sup>Pol<sup>-</sup> Charge Pairings, Also Known as “Intrinsic Sites,” and Pol<sup>+</sup>A<sup>-</sup> and Pol<sup>-</sup>M<sup>+</sup>, Extrinsic Sites (within Dotted Squares), Where Salt MA Acts as Counterions<sup>a</sup>**



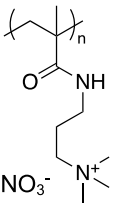
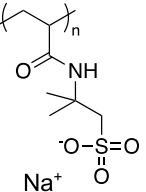
<sup>a</sup>Some salt ions within the PEC exist as co-ions (highlighted by dotted circles).

between charges.<sup>14,15</sup> A similar mechanism is often used to explain the control of Pol<sup>+</sup>Pol<sup>-</sup> interactions in PECs by MA.<sup>16–18</sup> An alternative approach focuses on a site-specific interplay between paired or unpaired units, connected via chemical equilibria.<sup>19,20</sup> Electrostatic theories take a step toward site-specificity by introducing charge–charge correlations.<sup>21,22</sup>

In the ideal specific salt “doping” model, one MA breaks one cross-link, as illustrated in Scheme 1. In fact, not all MA that enters a PEC breaks Pol<sup>+</sup>Pol<sup>-</sup> pairs (Scheme 1). Those that do so are termed counterions and those that do not are co-ions.<sup>23</sup> Though incorporated into theory,<sup>24</sup> to this point it has proven difficult to measure the fraction *f* of MA within the PEC acting as counterions. If *f* = 1, all salt within a PEC breaks charge pairs and the influence of physical cross-linking density on PEC properties such as linear viscoelastic response, LVR, could be reliably modeled.

Viscoelastic measurements of PECs yield critical information on the dynamics of these amorphous, hydrated materials.<sup>17,25–30</sup> Variables such as frequency and temperature, available to rheology, may be used to investigate modulus

**Table 1.  $M_w$ ,  $M_n$ ,  $\mathcal{D}$ , and  $n$  of the PMAPTA(NO<sub>3</sub>) and PAMPS Fractions<sup>a</sup>**

	$M_w$	$M_n$	$\mathcal{D}$	$n$	$N$
	kg mol <sup>-1</sup>	kg mol <sup>-1</sup>			
<b>PMAPTA(</b>	39.5	33.2	1.16	134	14
<b>NO<sub>3</sub>)</b>	181	168	1.09	679	72
	217	190	1.14	769	82
	349	319	1.09	1290	137
	390	356	1.10	1440	153
	613	554	1.11	2241	238
<b>PAMPS</b>	54.6	51.3	1.06	224	24
	139	128	1.09	559	60
	215	206	1.04	898	96
	270	248	1.09	1085	115
	370	347	1.06	1517	161
	502	472	1.06	2063	219

<sup>a</sup>*n* is the average number of monomers per polymer chain.  $n = M_n/M_0$ , and  $M_0$  the molecular weight of the monomer repeat unit: 247 g mol<sup>-1</sup> for MAPTA(NO<sub>3</sub>), and 229 g mol<sup>-1</sup> for AMPSNa and *N* the number of Kuhn segments

85 and viscosity as a function of molecular weight, and molecular  
86 weight distribution.<sup>31</sup> Many PECs exist in near-equilibrium  
87 with the “dilute phase” in which they are immersed and salt  
88 concentration is a reproducible and reversible variable.

89 The effects on phase compositions and LVR by reversibly  
90 breaking Pol<sup>+</sup>Pol<sup>-</sup> pairs using salt have been studied intensively  
91 over the past decade.<sup>26,32–36</sup> Polyelectrolyte pairs with  
92 matched molecular weights are optimal for studying chain  
93 relaxation dynamics. LVR for polymers exceeding the  
94 entanglement molecular weight,  $M_c$ , may be compared to  
95 theories for “sticky reptation,” which account for transient  
96 interactions between “sticker” groups.<sup>37–39</sup>

97 We have studied LVR for PECs below and above  $M_c$  using  
98 poly(methacrylic acid) salts, PMA, and poly([3-  
99 (methacrylamido)propyl]trimethylammonium chloride),  
100 PMAPTAC.<sup>40</sup> This pair forms a liquidlike PEC, far above  $T_g$   
101 at room temperature, which behaves like a polymer melt. Using  
102 carefully fractionated materials, time–temperature super-  
103 position produced LVR that was broad enough to show  
104 several classical crossovers in storage and loss modulus ( $G'$  and  
105  $G''$ , respectively) as a function of frequency. This work  
106 illustrated strong slowing of polymer dynamics on all scales but  
107 produced the unusual result that zero shear viscosity,  $\eta_0$ , scaled  
108 as  $N^5$  rather than  $N^3$  (predicted by theory).<sup>37,40</sup> Subsequent  
109 studies of PECs containing pH-sensitive (also termed “weak”)  
110 polyelectrolytes revealed a complex interplay between salt  
111 concentration, pH, and the degree of association and  
112 protonation within the PEC:<sup>41</sup> the presence of an oppositely  
113 charged polymer, or salt, shifts the apparent  $pK_a$ ,<sup>42</sup> which shifts  
114 the Pol<sup>+</sup>Pol<sup>-</sup> density.<sup>43</sup> Narrow molecular weight distribution  
115 polypeptides have been employed for many PEC sys-  
116 tems.<sup>33,36,44</sup> However, there is a wide range of LVR responses  
117 attributed to the hydrogen-bonding programmed into these  
118 biopolymers.<sup>45,46</sup>

119 Given the intense interest in PEC composition and  
120 dynamics, a good representative system is needed. The goals  
121 of the present work were to establish reliable LVR in a strongly  
122 charged, synthetic, liquidlike, entangled PEC, free of hydrogen  
123 bonding and made with narrow molecular weight distribution  
124 components. Comparison to theory places several additional  
125 demands on the system: first, PECs must be stoichiometric.  
126 Second, the chain dimensions and the “ideal monomer” Kuhn  
127 length, and whether this changes with temperature, must be  
128 measured. In addition, the mechanism for relaxation at the  
129 monomer length scale must be established. Finally, when salt is  
130 added to PECs, the fraction  $f$  that breaks charge pairs must be  
131 known so that the effective sticker density can be calculated.

## 132 ■ EXPERIMENTAL SECTION

133 **Materials.** [3-(Methacryloylamido)propyl]trimethylammonium  
134 chloride (MAPTAC, 50 wt % in H<sub>2</sub>O), 2-acrylamido-2-methyl-1-  
135 propanesulfonic acid sodium salt (AMPS, 50 wt % in H<sub>2</sub>O), N-(3-  
136 aminopropyl)methacrylamide hydrochloride (AMA), dimethylforma-  
137 mide (DMF), *d*<sub>3</sub>-iodomethane (CD<sub>3</sub>I), ethyl acetate, 1,2,2,6,6-  
138 pentamethylpiperidine (PMP), inhibitor removal beads, sodium  
139 nitrate (NaNO<sub>3</sub>), sodium azide (NaN<sub>3</sub>), and sodium thiocyanate  
140 (NaSCN) were from Sigma-Aldrich. Acetone used for fractionation  
141 and polymer purification was from Fisher Chemicals. Deuterium  
142 dioxide (D<sub>2</sub>O, 99.9%) was from Cambridge Isotope laboratories. The  
143 radioactive salts were sodium chloride (<sup>22</sup>NaCl, 54.3  $\mu$ Ci) from  
144 PerkinElmer and potassium thiocyanate (K<sup>14</sup>CN, 100  $\mu$ Ci) from  
145 ViTrax. Ultrapure water (18.2 M $\Omega$  cm) was supplied via a Barnstead  
146 E-Pure system (Thermo Scientific) to prepare all solutions.

**Polymer Synthesis.** Solutions of MAPTAC and AMPS 147  
monomers were stirred for 4 h with inhibitor removal beads. After 148  
filtering out the beads, 50 mL of MAPTAC solution was diluted with 149  
water to a concentration of 1.19 M. A similar dilution with AMPS 150  
yielded 1.46 M AMPS. 8 mg of K<sub>2</sub>S<sub>2</sub>O<sub>8</sub> initiator was added to the 151  
solutions, and free radical polymerization was carried out at 65 °C 152  
under N<sub>2</sub> and stirring for 18 h. The polymer solutions were freeze- 153  
dried and then dried at 120 °C for 18 h. 154

**Polyelectrolyte Fractionation.** To isolate polyelectrolyte (PE) 155  
samples with low dispersity, molecular weight fractionation was 156  
carried out with the starting PMAPTAC ( $M_w = 311$  kg mol<sup>-1</sup>,  $\mathcal{D} = 157$   
2.32) and PAMPS ( $M_w = 119$  kg mol<sup>-1</sup>,  $\mathcal{D} = 1.71$ ) samples. Acetone 158  
was gradually added to 10 g of PMAPTAC or PAMPS in 100 mL of 159  
water. Each fraction precipitating out was collected by centrifuging 160  
the solution at 6000 rpm for 30–60 min. Additional acetone was 161  
added to the remaining polymer solution, and the process was 162  
repeated to obtain several fractions. The fractions were dried at 120 163  
°C for 18 h. Unless otherwise stated, PMAPTA/PAMPS PECs were 164  
made with the  $\mathcal{D} = 2.32/1.71$  mentioned above. 165

**Size Exclusion Chromatography (SEC).** Size exclusion 166  
chromatography (Supporting Information Figure S1) was used to 167  
determine the weight-average molecular weight,  $M_w$ , number-average 168  
molecular weight,  $M_n$ , and the dispersity index ( $\mathcal{D} = M_w/M_n$ ), all given 169  
in Table 1. Molecular weights include the counterions of the mobile 170  
phase (see the Supporting Information for a detailed procedure). 171

**Preparing Stoichiometric Polyelectrolyte Complexes.** Nearly 172  
stoichiometric PECs were prepared by mixing equimolar solutions 173  
(0.125 M) of PMAPTAC and PAMPS in 0.1 M NaSCN. The mixture 174  
was stirred for an hour at room temperature, and the polymer-rich 175  
phase (PEC) was collected. The PEC was rinsed in water to wash out 176  
the salt ions and then dried for 18 h at 120 °C. The ratio of 177  
PMAPTA:PAMPS was measured using NMR (Supporting Informa- 178  
tion Figure S2) and verified by radiolabeling (see below). For NMR, 179  
10 mg of sample was dissolved in 1.0 mL, 1.0 M NaSCN in D<sub>2</sub>O (for 180  
PMAPTAC or PAMPS homopolymers) while the complexes were 181  
dissolved in 0.6 M NaSCN in D<sub>2</sub>O, and <sup>1</sup>H NMR spectra were 182  
collected using an AVANCE 600 MHz NMR (Bruker). All PECs were 183  
liquidlike and transparent. 184

**Radiolabeling.** The degree of nonstoichiometry can be precisely 185  
measured by determining the amount of residual counterions. Excess 186  
charge from either polyelectrolyte will be compensated by a 187  
counterion (Na<sup>+</sup> compensates excess AMPS<sup>-</sup> and SCN<sup>-</sup> compensates 188  
excess MAPTA<sup>+</sup>). Unlabeled counterions were replaced with labeled 189  
ones by soaking the PEC in a dilute solution of radiolabeled ions 190  
(NaS<sup>14</sup>CN or <sup>22</sup>NaSCN) as in prior work (see the Supporting 191  
Information for detailed procedure). The number of moles of PEC, 192  
<sup>22</sup>Na<sup>+</sup>, and S<sup>14</sup>CN<sup>-</sup> in the PEC are given in Table 2. 193

**Table 2. Stoichiometry of P1479 PEC via Radiolabeling**

P1479 (mol repeat units)	$1.52 \times 10^{-4}$
S <sup>14</sup> CN <sup>-</sup> PEC (mol)	$3.27 \times 10^{-6}$
<sup>22</sup> Na <sup>+</sup> PEC (mol)	$5.12 \times 10^{-7}$
Pol <sup>+</sup> /Pol <sup>-</sup>	1.018

A small amount of salt enters the PEC via doping, which introduces 194  
both Na<sup>+</sup> and SCN<sup>-</sup>. Excess Pol<sup>+</sup> only brings in SCN<sup>-</sup>. The 195  
stoichiometry is given by 196

$$\frac{[\text{Pol}^+]}{[\text{Pol}^-]} = 1 + \frac{\text{moles of SCN}^- - \text{moles of Na}^+}{\text{moles of PEC}} \quad (1) \quad 197$$

**Critical Salt Concentration (CSC).** Turbidimetry was used to 198  
determine the CSC. A Cary 100 UV–visible spectrophotometer 199  
(Varian) was used to measure the absorbance of 1 mg mL<sup>-1</sup> solutions 200  
of PMAPTA/PAMPS at  $\lambda = 450$  nm. 0.025 g of dry PEC was 201  
dissolved in 25 mL of 0.6 M NaSCN. Solutions with  $n_{\text{avg}} = 1188, 834,$  202  
and 179 were prepared and their absorbances measured as the 203  
concentration of NaSCN was varied near the PEC CSC, which was 204  
determined to be between 0.5 and 0.6 M NaSCN by visual inspection 205

206 of the point at which sufficient NaSCN had been added to dissolve  
207 the PEC. 2 mL of each dissolved PEC solution was diluted with  
208 aliquots of 100  $\mu\text{L}$   $\text{H}_2\text{O}$  until the absorbance increased to above 1  
209 (“reverse” method). 100  $\mu\text{L}$  of  $[\text{NaSCN}] = 0.6 \text{ M}$  was then gradually  
210 added to increase the concentration back to above the CSC  
211 (“forwards” method), until the solution no longer scattered light  
212 (absorbance  $\approx 0$ ).

213 **Doping Behavior.** The composition, including the concentration  
214 of salt in the PEC,  $[\text{NaSCN}]_{\text{PEC}}$ , as a function of the concentration of  
215 salt in solution (dilute phase),  $[\text{NaSCN}]_{\text{s}}$ , was determined by soaking  
216 a known mass of dry PMAPTA/PAMPS in different  $[\text{NaSCN}]_{\text{s}}$  (0.3,  
217 0.2, 0.1, 0.08, 0.06, 0.04, 0.02, 0.01 M), removing the supernatant,  
218 then releasing the PEC salt ions into 110 mL water in a jacketed,  
219 temperature-controlled cell and recording the conductivity using a  
220 four-probe conductivity cell (Orion 013005MD, Thermo Scientific)  
221 and a conductivity meter (Orion 3 star, Thermo Scientific). The  
222 conductivity at long time,  $\sigma_{\infty}$ , assumed to correspond to the release of  
223 all salt in the PEC, was converted to the salt content using  
224 conductivity standards. The water content was determined from the  
225 mass of the hydrated PEC in the various  $[\text{NaSCN}]_{\text{s}}$ . The conductivity  
226 cell was thermostated to  $\pm 0.1 \text{ }^\circ\text{C}$  with a Thermo Haake K20  
227 circulator and stirred with a large paddle.

228 **Linear Viscoelastic Response.** The storage modulus  $G'$ , loss  
229 modulus,  $G''$ , and complex viscosity,  $\eta$ , for the PEC pairs were  
230 evaluated as a function of temperature and salt concentration using a  
231 stress-controlled DHR-3 rheometer (TA Instruments). PEC pairs  
232 P179, P619, P834, P1188, P1479, P2152, P1, and P2 (details given in  
233 Table 3) were soaked in 0.01 M NaSCN for a minimum of 18 h,

**Table 3. Pairs of PMAPTA and PAMPS with Matched, or Mismatched, Chain Lengths<sup>a</sup>**

$P_{\text{nav}}$	$n_{\text{av}}$	$N^+$	$N^-$	$N_{\text{av}}$	Pol <sup>+</sup> /Pol <sup>-</sup>
P179	179	14.3	23.8	19.1	0.97:1
P619	619	72.2	59.4	65.9	0.98:1
P834	834	81.8	95.5	88.7	0.98:1
P1188	1188	137	115	126	0.97:1
P1479	1479	153	161	157	0.99:1
P2152	2152	238	219	229	0.98:1
P1	239	24			0.96:1
P2	15	219			1:1.02

<sup>a</sup>The average number of Kuhn segments ( $N_{\text{av}}$ ) in the PMAPTA/PAMPS pairs. Mole ratio of PMAPTA<sup>+</sup>:PAMPS<sup>-</sup> measured by NMR. P179 was below entanglement. P1 and P2 were mismatched lengths.

234 loaded onto the lower plate of the rheometer, and compressed using a  
235 20 mm upper plate while immersed in 0.01 M NaSCN using a  
236 reservoir built in-house. The reservoir was equipped with a lid to  
237 prevent evaporation. The storage and loss modulus were recorded as a  
238 function of oscillation frequency across a range of temperatures  
239 (between  $-5$  and  $85 \text{ }^\circ\text{C}$ ) at 0.1% strain, well within the linear  
240 viscoelastic regime. Time-temperature superposition (TTS) was  
241 performed to obtain responses at a reference temperature  $T_r = 25 \text{ }^\circ\text{C}$   
242 across a wide range of effective frequencies ( $10^{-4}$ – $10^5 \text{ rad s}^{-1}$ ).

243 For zero shear viscosities, the steady state viscosity was recorded as  
244 a function of shear rate at  $55 \text{ }^\circ\text{C}$  using the lowest range of shear rates  
245 available ( $10^{-4}$ – $10^{-2} \text{ rad s}^{-1}$ ). The system was given 180 s to reach  
246 equilibrium after applying a shearing force. Viscosity independent of  
247 shear rate gave a plateau of values, which were averaged across the  
248 plateau to yield  $\eta_0$ , zero shear viscosity, as a function of molecular  
249 weight and salt concentrations (for the pair  $n_{\text{av}} = 1479$ ).

250 **FTIR Spectroscopy.** Attenuated total internal reflection Fourier  
251 transform infrared spectroscopy (ATR-FTIR) was used to monitor  
252 the absorbances corresponding to the  $\text{C}\equiv\text{N}$  stretch for thiocyanate  
253 (at  $2060 \text{ cm}^{-1}$  when  $\text{SCN}^-$  is a counterion and  $2064 \text{ cm}^{-1}$  when it is a  
254 co-ion). Spectra of 0.6 M aqueous NaSCN, 1.0 M PMAPTA<sup>+</sup> with  
255  $\text{SCN}^-$  as counterion (PMAPTA(SCN)), 1.0 M PAMPS dissolved in  
256 0.6 M NaSCN, and PMAPTA/PAMPS PEC doped in 0.3 M NaSCN

were collected at  $0.5 \text{ cm}^{-1}$  resolution using a Thermo Scientific 257  
Nicolet iS20 with a Pike MIRacle ATR attachment fitted with a 258  
single-reflection diamond/ZnSe crystal. The background for all 259  
measurements was air. PMAPTA(SCN) was obtained via ion 260  
exchange by dialyzing a dilute solution of PMAPTAC against 261  
NaSCN (see above). 262

**Measuring Ion Diffusion.** The diffusion coefficient,  $D_{\text{ions}}$  ( $\text{cm}^2$  263  
 $\text{s}^{-1}$ ), of NaSCN in PMAPTA/PAMPS was measured as a function of 264  
temperature using the kinetics of salt release from the PEC into a 265  
solution of fresh water over a temperature range of  $5$ – $65 \text{ }^\circ\text{C}$ . 1.43 g of 266  
hydrated PMAPTA/PAMPS soaked in 0.10 M NaSCN, 0.066 cm 267  
thickness and 2.5 cm radius, was placed inside a water-jacketed beaker 268  
connected to a circulating thermostat. 110 mL water, equilibrated at 269  
the target temperature, was poured over the coacervate disk at  $t = 0$  270  
and the conductivity was recorded every 10 s until a plateau was 271  
reached. To ensure kinetics of salt release were limited by diffusion 272  
through the PEC, and not by diffusion through solution, the solution 273  
above the PEC was briskly stirred with a large paddle. 274

The tracer diffusion coefficient of  $\text{SCN}^-$ ,  $D_{\text{SCN}^-}$ , within PECs 275  
doped with  $[\text{NaSCN}]_{\text{s}} = 0.01, 0.02, 0.04, 0.08, 0.16,$  and  $0.3 \text{ M}$  was 276  
measured at room temperature ( $T = 23.4 \text{ }^\circ\text{C}$ ) by self-exchange of 277  
labeled ( $\text{S}^{14}\text{CN}^-$ ) with unlabeled  $\text{SCN}^-$ . 0.15 g of dry PMAPTA/ 278  
PAMPS was added to 10 mL of each salt concentration (starting with 279  
0.01 M NaSCN) and 10  $\mu\text{L}$  of  $\text{NaS}^{14}\text{CN}$  (1  $\mu\text{Ci}$ , 1 Ci =  $3.7 \times 10^{10}$  280  
disintegrations per second) was added. 24 h was allowed for the 281  
radioisotope to exchange into the PEC. The kinetics of  $\text{SCN}^-$  release 282  
was measured by removing the radioactive solution and substituting it 283  
with an unlabeled NaSCN solution of the same concentration. 284  
Maintaining vigorous stirring, 100  $\mu\text{L}$  aliquots were extracted at 285  
different times, mixed with 2 mL liquid scintillation cocktail and the 286  
counts were recorded using the  $^{14}\text{C}$  channel of the scintillation 287  
counter until the count rate of sequential aliquots reached a plateau. 288

**Small-Angle Neutron Scattering (SANS).** The syntheses of 289  
deuterated monomer and polymer are described in the Supporting 290  
Information. The deuterated polymer was fractionated as above into 291  
samples with defined size and paired with a polyelectrolyte with 292  
matching degree of polymerization (Table 4, Figure S3, Table S1). A 293 14  
1:4 mol ratio mixture of deuterated and nondeuterated PMAPTAC 294  
was complexed with PAMPS under stoichiometric conditions. 295

**Table 4. Number of Repeat Units in PMAPTA<sup>+</sup> ( $n^+$ ), Number of Repeat Units in PAMPS<sup>-</sup> ( $n^-$ ), and Number of Repeat Units in the Deuterated PMAPTA<sup>+</sup> ( $n^{\text{D}+}$ ) Comprising the Samples Used in Neutron Diffraction**

PEC	$n^+$	$n^{\text{D}+}$	$n^-$
d-A	1290	1363	1085
d-B	739	609	559

Nondeuterated components were contrast-matched using a 1:4 296  
 $\text{D}_2\text{O}/\text{H}_2\text{O}$  mixture. Scattering length densities (SLDs) of one 297  
PMAPTA/PAMPS unit ( $\text{C}_{17}\text{H}_{33}\text{N}_3\text{O}_8\text{S}$ ) at different  $\text{D}_2\text{O}/\text{H}_2\text{O}$  ratios 298  
were matched with the appropriate 0.1 M NaSCN  $\text{D}_2\text{O}/\text{H}_2\text{O}$  mixture 299  
of equal SLD. The SLDs were calculated using the NIST online 300  
calculator (density =  $1.1 \text{ g cm}^{-3}$ , sample thickness = 1 mm, and 301  
neutron wavelength of 6  $\text{\AA}$ ). PECs d-A and d-B were soaked in 0.1 M 302  
NaSCN/1:4  $\text{D}_2\text{O}/\text{H}_2\text{O}$  and annealed at  $50 \text{ }^\circ\text{C}$  for 18 h. The 303  
complexes were then loaded into 1 mm path 20 mm diameter silica 304  
banjo cells, sealed while covered with the contrast-matched solvent, 305  
and annealed at  $45 \text{ }^\circ\text{C}$  for 3 days. The samples were slowly cooled 306  
back to room temperature. SANS measurements were performed on 307  
the extended  $q$ -range small-angle neutron scattering diffractometer 308  
(EQ-SANS) at the Spallation Neutron Source (SNS) at Oak Ridge 309  
National Laboratory (ORNL). Two sample-to-detector distances (9 310  
and 4 m) in combination of wavelength bands defined by minimum 311  
wavelength of 15 and 2.5  $\text{\AA}$ , respectively, were used to cover the  $q$ - 312  
range of  $0.003 \text{ \AA}^{-1} < q < 0.3^{-1}$ , where the magnitude of the scattering 313  
vector,  $q$ , is defined by  $q = (4\pi/\lambda)\sin(\theta)$ . Here,  $\lambda$  is the wavelength of 314  
neutron and  $2\theta$  is the scattering angle. Absolute scale intensities were 315

316 calibrated with a porous silica standard sample. Measurements were  
 317 performed at 25 °C for samples d-A and d-B, and a reference banjo  
 318 cell loaded with the contrast-matched electrolyte. Sample d-B was also  
 319 measured at 35, 45, and 65 °C. The data reduction including  
 320 corrections for detector sensitivity and background was performed  
 321 using MantidPlot software. SasView was used to fit the data to the  
 322 scattering intensity versus  $q$  for a monodisperse Gaussian coil.

## 323 ■ RESULTS

324 SANS was used to evaluate the radius of gyration,  $R_g$ , of D-  
 325 PMAPTA in PMAPTA/PAMPS, and thence the length of a  
 326 statistical Kuhn unit.  $R_g$  was measured for two PECs of  
 327 different chain lengths and as a function of temperature. D-  
 328 PMAPTAI (see Figure S3 and Table S1) was used to make a  
 329 deuterium-labeled PEC by mixing 25 mol % P(D-MAPTAI)  
 330 with 75 mol % PMAPTAC, and PAMPS in stoichiometric  
 331 ratios to obtain complexes with polymer chain lengths given in  
 332 Table 4. Dilution of the deuterated chains in this way simplifies  
 333 the analysis by separating interchain from intrachain  
 334 correlations.<sup>47</sup> To ensure that the deuterated polymers were  
 335 the only segments contributing to coherent scattering, the  
 336 nondeuterated components were contrast-matched with a 1:4  
 337 mixture of D<sub>2</sub>O and H<sub>2</sub>O. Figure 1 shows the neutron  
 338 scattering profile from the two PEC samples (see also Figure  
 339 S4) soaked in a 0.1 M NaSCN 1:4 D<sub>2</sub>O/H<sub>2</sub>O solution.

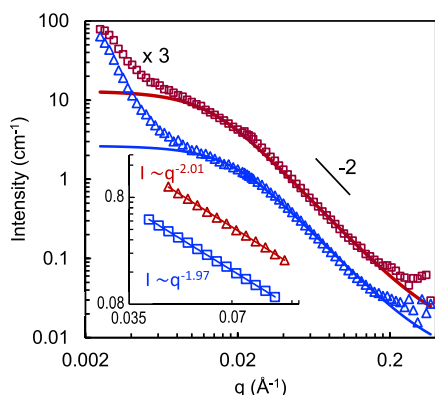


**Figure 1.** Small-angle neutron scattering of PEC d-A (upper curve,  $n_{\text{DMAPTA}} = 1363$ , Table 4) displaced for clarity by a factor of 3 and PEC d-B (lower curve  $n_{\text{DMAPTA}} = 609$ , Table 4), both in 0.10 M NaSCN at 25 °C. 25% of the PMAPTA was pure D-MAPTA homopolymer. The nondeuterated components were contrast-matched with a mixture of 1:4 D<sub>2</sub>O/H<sub>2</sub>O. The fits (solid lines) are to Gaussian coils with respective  $R_g$  of 11.3 and 8.0 nm. The inset shows the Guinier region: intensity from 0.08 to 0.8 and  $q$  from 0.04 to 0.09 Å<sup>-1</sup>.

340 In intermediate  $q$  ranges ( $0.02 \text{ \AA}^{-1} < q < 0.2 \text{ \AA}^{-1}$ ), the  
 341 scattering is predominantly from length scales of the polymer  
 342 coil size (D-PMAPTA in this case). SASview was used to fit  
 343 the form factor,  $P(q)$  for Gaussian chains

$$344 \quad P(q) = \frac{2(e^{-x} + x - 1)}{x^2} \quad (2)$$

345 where  $x = q^2 R_g^2$ . The scattering intensity  $I(q)$  decays with  $q$  as  
 346  $I(q) \sim q^{-2}$  (Figure 1, inset; Figure S4) which is a feature of  
 347 scattering from Gaussian chains. The  $R_g$  measured for PECs d-  
 348 A and d-B was 11.3 and 8.0 nm, respectively. The Kuhn length,  
 349  $b$ , was calculated from the polymer contour length  $nl$  ( $n$  is the  
 350 number of monomer repeat units and  $l = 0.252$  nm is the  
 351 length between repeat units along the backbone) such that  $b =$

$6R_g^2/nl$ .  $b$  was determined to be 2.23 and 2.50 nm for the 352  
 longer and shorter chains in Figure 1, respectively, for an 353  
 average of  $2.37 \pm 0.19$  nm. The Kuhn length for PAMPS in a 354  
 $\theta$ -solvent was reported to be 2.4 nm.<sup>48</sup> The number of 355  
 monomer units,  $n_K$ , in a Kuhn length is  $b/l = 9.4$ . Scattering 356  
 from PEC d-B ( $n_{\text{DMAPTA}} = 609$ ) over the same  $q$ -range was 357  
 measured as the system was heated (5–65 °C, Figure S4) and 358  
 the fitted  $R_g$  was found to be constant within error ( $8.0 \pm 0.20$  359  
 nm) as a function of temperature. 360

**Critical Salt Concentration, CSC.** Sufficiently concen- 361  
 trated salt solutions swell, then dissolve, most PECs, effectively 362  
 reversing the liquid–liquid phase separation that caused 363  
 them.<sup>49</sup> The point at which this occurs, often judged by eye, 364  
 or measured with turbidimetry, is the CSC (also termed “salt 365  
 resistance”<sup>50</sup>). The CSC, a readily accessible point on the 366  
 phase diagram of PECs in equilibrium with the dilute phase, 367  
 depends on molecular weight: the CSC for shorter chains is 368  
 lower.<sup>23</sup> The CSC also depends strongly on the chemical 369  
 nature of MA: salts containing ions at the hydrophobic end of 370  
 the Hofmeister series are more effective at dissolving PECs. 371  
 Some PECs which do not show an apparent CSC at any [MA]<sub>s</sub> 372  
 for a particular salt may be dissolved with a more hydrophobic 373  
 salt.<sup>41</sup> The CSCs for three PMAPTA/PAMPS pairs in NaSCN 374  
 are shown in Figure 2. 375

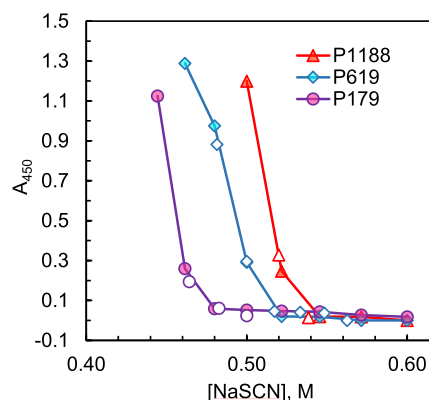
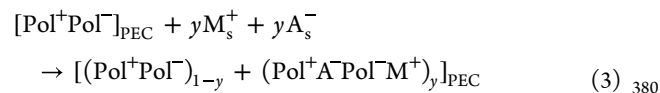


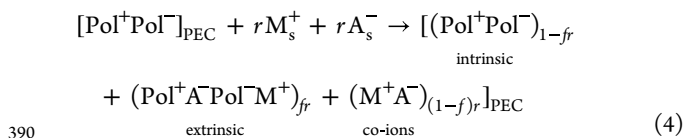
**Figure 2.** Measurement of the critical salt concentration of 1 mg mL<sup>-1</sup> PMAPTA/PAMPS using PECs P179 (circles); P619 (diamonds); and P1188 (triangles) pairs, all with low polydispersity (see Tables 1 and 3). Turbidity is given by the absorbance at a wavelength of 450 nm ( $A_{450}$ ) at room temperature. The CSC is taken to be  $[\text{NaSCN}]_c$ , where  $A_{450}$  drops to zero. First, 0.6 M NaSCN was added to 3 mg of PEC, which was slightly above  $[\text{NaSCN}]_{\text{S,CSC}}$  (absorbance  $\approx 0$ ). Water was then added to dilute the NaSCN and bring the solution below the  $[\text{NaSCN}]_{\text{S,CSC}}$  in the “desalting” or “reverse” method (filled symbols). Then, NaSCN was added to the precipitated PEC to dissolve it again (the “forwards” method, open symbols).

**Specific Doping of PEC by NaSCN.** Below the CSC, MA 376  
 added to solution is assumed to “dope” the PEC, represented 377  
 by eq 3, in a site-specific model. (In contrast, MA “shields” the 378  
 polymer charges in continuum electrostatics models) 379



where  $y$  is the fraction of intrinsic sites converted to extrinsic 381  
 ones, “s” is the solution phase, and “PEC” is the PEC phase. 382  
 Equation 3 assumes all salt in the PEC breaks  $\text{Pol}^+\text{Pol}^-$  pairs, 383  
 as in Scheme 1. However, it has been found experimentally<sup>23,51</sup> 384

385 and computationally<sup>24</sup> that MA does not necessarily break  
386 Pol<sup>+</sup>Pol<sup>-</sup> pairs and, especially near the CSC,<sup>34</sup> much of the salt  
387 exists as co-ions rather than the counterions implied by eq 3. A  
388 more accurate representation of the disposition of ions within a  
389 PEC is



where  $r$  is the molar ratio of total MA in the PEC to Pol<sup>+</sup>Pol<sup>-</sup>  
and  $f$  is the fraction of MA within the PEC acting as  
counterions. Thus,  $y = fr$ . Figure 3 shows  $r$  as a function of

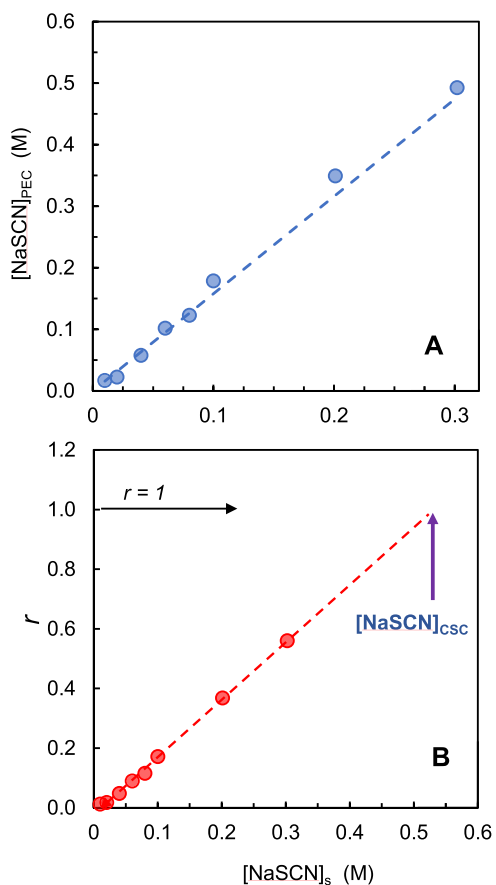
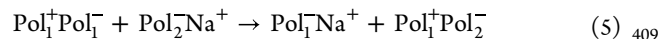


**Figure 3.** Doping of PMAPTA/PAMPS PEC with NaSCN at room temperature. (A) Molar concentration of NaSCN in the PEC, [NaSCN]<sub>PEC</sub>, as a function of [NaSCN]<sub>s</sub> in the solution or “dilute phase,” [NaSCN]<sub>s</sub>. The dashed line is provided by eq 10, where  $f$  was assumed to be 1 and  $\Delta H_{\text{PEC}}$  was measured to be +2255 J mol<sup>-1</sup>; [NaSCN]<sub>PEC</sub> = 1.58[NaSCN]<sub>s</sub>. (B) Ratio  $r = [\text{NaSCN}]_{\text{PEC}}/[\text{PE}]_{\text{PEC}}$  versus [NaSCN]<sub>s</sub>. The dotted line gives  $r = 1.93[\text{NaSCN}]_s - 0.02$ . From this fit, at  $r = 1$ , [NaSCN]<sub>s</sub> = 0.53 M, which is close to the experimental CSC (Figure 2).

394 [NaSCN]<sub>s</sub>. The data is also presented as [NaSCN]<sub>PEC</sub> versus  
395 [NaSCN]<sub>s</sub>, which makes it clear that the concentration of MA  
396 in the PEC is more than that in the supernatant at equilibrium,  
397 in conflict with most electrostatics-based theory.<sup>10</sup> As with  
398 most PEC doping responses,<sup>23,51</sup> there is a small intercept on  
399 the [MA]<sub>s</sub> axis, giving a negative intercept on the  $r$  axis (here,  
400 about -0.02), probably due to a combination of the residual  
401 ions from excess PMAPTA<sup>+</sup> (about 2%) and the osmotic

pressure of the chains themselves. These nonidealities are hard  
to avoid,<sup>27</sup> as all undoped PECs contain a few extrinsic sites  
(see Table 3), making it difficult to approach truly ion-free  
PEC.

**Ion Dynamics as a Reporter of Polymer Repeat Unit Dynamics.** Ion transport in PECs can be modeled by hopping between adjacent segments of the same charge,<sup>40</sup> e.g.,



Because counterion dynamics are coupled to, and limited by, polymer dynamics,<sup>52</sup> the ion hopping rate  $\omega_{\text{ion}}$  is assumed to be the same as the Pol<sup>+</sup>Pol<sup>-</sup> breaking rate.<sup>40</sup> The diffusion coefficient of NaSCN was determined by monitoring the conductivity of a solution of fresh water which was poured on top of a doped PEC film. The fraction of the released salt ( $\psi = M_{\text{NaSCN}_t}/M_{\text{NaSCN}_{t\infty}}$ ), where  $M_{\text{NaSCN}_t}$  is the amount of NaSCN released at time  $t$ , was used to evaluate the salt diffusion coefficient,  $D_{\text{ions}}$  of NaSCN (cm<sup>2</sup> s<sup>-1</sup>) using the equation for diffusion out of/into a plate<sup>53</sup>

$$\begin{aligned}
 \psi &= \frac{M_t}{M_\infty} \\
 &= 1 - \sum_{n=0}^{\infty} \frac{8}{(2n+1)^2\pi^2} \exp\left[-\frac{D_{\text{ions}}(2n+1)^2\pi^2 t}{4\sigma^2}\right] \\
 &= \left(\frac{2\sqrt{D_{\text{ions}}t}}{\sigma\sqrt{\pi}}\right)_{\psi < 0.6} \quad (6)
 \end{aligned}$$

where  $\sigma$  is the thickness of the PEC. The boundary conditions for eq 6 are diffusion from one side of a parallel plate, assume uniform distribution of ions in the PEC at  $t = 0$ , and the concentration of ions at the surface and in the bulk water  $\rightarrow 0$ , ensured by a large volume of water and brisk stirring at the interface. The slope of the line in Figure 4A is the linear limit of eq 6, valid for  $\psi < 0.6$ . Average ion hopping frequencies can then be calculated by assuming three-dimensional hopping between nearest neighbors

$$\omega_{\text{ion}} = \frac{6D_{\text{ions}}}{d^2} \quad (7)$$

where  $d$  is the hopping distance or the distance between Pol<sup>+</sup>Pol<sup>-</sup> pairs (Table S2). The relaxation rate slows with cooling according to the Arrhenius equation with activation energy  $E_i$  (J mol<sup>-1</sup>)

$$\omega_{\text{ion}} = A_1 e^{-E_i/RT} \quad (8)$$

$E_i$  was calculated from the slope of  $\ln D$  vs  $1/T$  to be 18.2 kJ mol<sup>-1</sup> and  $A_1$  was found from the intercept of Figure 4B:  $1.36 \times 10^{12}$  s<sup>-1</sup>.

The tracer diffusion coefficient of SCN<sup>-</sup>,  $D_{\text{SCN}}$ , at different [NaSCN]<sub>s</sub> was determined by measuring the fraction of radioactive thiocyanate, S<sup>14</sup>CN<sup>-</sup>, released into a solution of nonradioactive NaSCN of the same concentration (Figure 5).  $D_{\text{SCN}}$  remained surprisingly similar (Figure 5B) over the range of [NaSCN]<sub>s</sub>, another indication that SCN<sup>-</sup> clings to MAPTA<sup>+</sup> as it hops through the PEC. In fact, the only reason for the variation of  $D_{\text{SCN}}$  is from the slight increase in film thickness  $\sigma$  as the PEC is doped. There is little evidence that NaSCN accelerates dynamics by “screening” Pol<sup>+</sup>Pol<sup>-</sup> electrostatic interactions.<sup>17</sup>

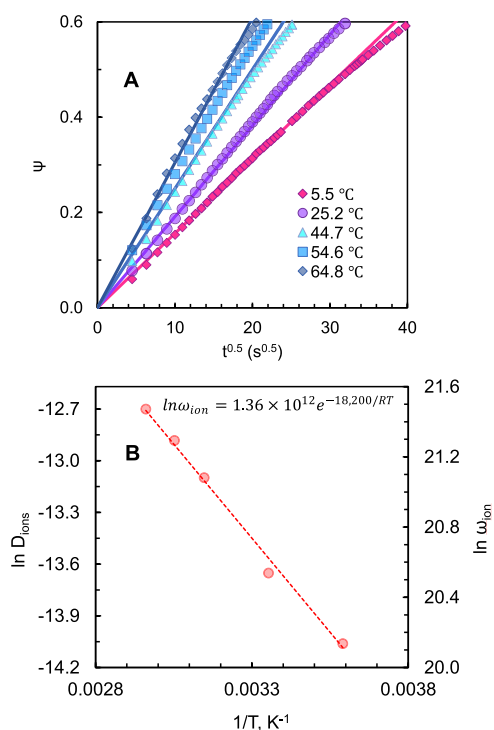


**Figure 4.** (A) Fraction  $\psi$  of NaSCN released into water as a function of  $t^{0.5}$  ( $s^{0.5}$ ) at various temperatures from a PMAPTA/PAMPS PEC doped in 0.1 M NaSCN. Solid lines are the fit to eq 6 using the fitted diffusion coefficients ( $\text{cm}^2 \text{s}^{-1}$ ) in (B) (left axis). The hopping frequencies were calculated using  $\omega_{\text{ion}} = \frac{6D_{\text{ions}}}{d^2}$  and an average distance  $d$  between  $\text{Pol}^+\text{Pol}^-$  pairs of  $0.95 \times 10^{-7}$  cm (in 0.1 M NaSCN, Table S2). The slope gives an activation energy of 18.2  $\text{kJ mol}^{-1}$  and an intercept  $D_0$  of  $2.05 \times 10^{-3} \text{ cm}^2 \text{ s}^{-1}$  and  $A_1 = 1.36 \times 10^{12} \text{ s}^{-1}$ .

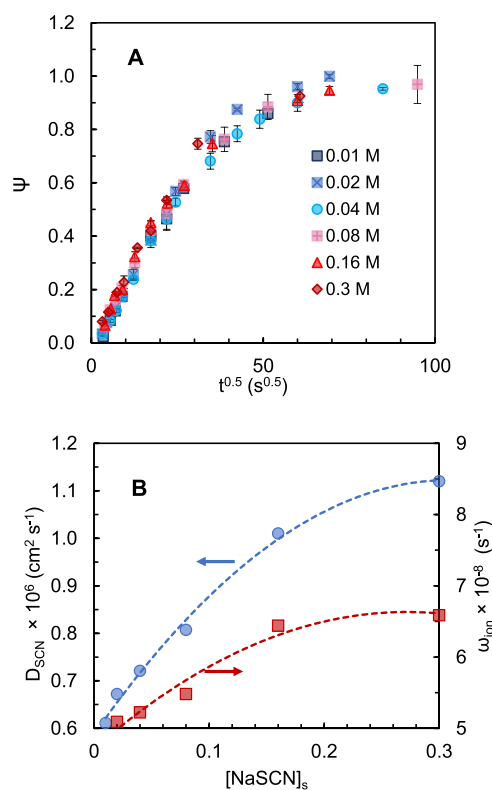


**Figure 5.** (A) Fraction of radiolabeled  $\text{S}^{14}\text{CN}^-$ ,  $\psi$ , exchanged with 10 mL of unlabeled NaSCN as a function of time  $t^{0.5}$  ( $s^{0.5}$ ) at  $[\text{NaSCN}]_s = 0.01, 0.02, 0.04, 0.08, 0.16,$  and  $0.3$  M. Room temperature. (B) Diffusion coefficient fits to eq 6 for  $\psi < 0.6$  as a function of  $[\text{NaSCN}]_s$  (blue circles). Ion hopping frequencies were calculated from eq 7 using  $d$  values given in Table S2 (red squares). The dotted lines are a guide to the eye.

450  $D_{\text{ions}}$  represents the coupled diffusion coefficient between  
451  $\text{Na}^+$  and  $\text{SCN}^-$ , while  $D_{\text{SCN}}$  is the tracer or single ion  
452 coefficient for  $\text{SCN}^-$ . The two are related by<sup>54</sup>

$$D_{\text{ions}} = \frac{2D_{\text{Na}}D_{\text{SCN}}}{D_{\text{Na}} + D_{\text{SCN}}} \quad (9)$$

454 where  $D_{\text{Na}}$  is the tracer diffusion coefficient for  $\text{Na}^+$ . Because  
455 the coefficients at 25 °C for  $D_{\text{ions}}$  and  $D_{\text{SCN}}$  are similar ( $1.3 \times$   
456  $10^{-6}$  and  $1.0 \times 10^{-6} \text{ cm}^2 \text{ s}^{-1}$ , respectively),  $D_{\text{Na}}$  must be close  
457 to  $D_{\text{SCN}}$ .

458 **Linear Viscoelastic Response (LVR).** Rheology was used  
459 the monitor the LVR of PEC pairs of various lengths. The  
460 storage and loss modulus were measured at a strain of 0.1%  
461 and at different temperatures in the frequency range  $0.01 < \omega$   
462  $< 100 \text{ rad s}^{-1}$ . Time–temperature superposition, TTS, was  
463 used to study the dynamics across a wider range of frequencies  
464 in Figure 6. Individual TTS plots of the pairs along with shift  
465 factors  $a_T$  and  $b_T$  are given in Figure S5.

466 Figure 6B gives  $G'$  and  $G''$  for pairs P619, P834, 1188,  
467 P1479, and P2152, all above entanglement as indicated by the  
468 two dynamic crossover points at lower frequencies:  $\omega_{\text{rep}}$  and  
469  $\omega_e$ .  $\tau_{\text{rep}} = 1/\omega_{\text{rep}}$  describes the relaxation time of the longest  
470 dynamic length scale corresponding to a polymer chain  
471 reptating out of a tube.

472 Table 5 summarizes the characteristic LVR parameters for  
473 PEC pairs. Characteristic relaxation times are read directly  
474 from the  $G'$  and  $G''$  crossing points in Figure 6: reptation time,

$\tau_{\text{rep}}$ ; Rouse relaxation time of a chain length between  
475 entanglements,  $\tau_e$ ; relaxation time of a Kuhn (ideal) monomer,  
476  $\tau_0$ . Plateau modulus  $G_0$  was taken as  $G'$  at the maximum of  $G'/$   
477  $G''$  (minimum of  $\tan \delta$ ). The number of Kuhn monomers  
478 between entanglements,  $N_e = M_e/M_0n_K$ , where  $M_e$  was  
479 calculated from eq 11. 480

## DISCUSSION

481  
482 In order to understand the response of PECs to variables such  
483 as temperature, molecular weight, and salt concentration, many  
484 parameters must be known, including the coil size, and the  
485 dependence of coil size on temperature. This work attempts to  
486 measure these on the same, well-behaved system to enable  
487 theoretical and quantitative descriptions. Because charged  
488 monomers were used for synthesis, the resulting polyelec-  
489 trolytes were fully charged. PMAPTAC and PAMPS yield a  
490 liquid-like PEC well above  $T_g$  at room temperature, similar to  
491 conditions used for many neutral polymers to probe dynamics  
492 in the melt phase. The quaternary ammonium and sulfonate  
493 charged groups on the respective polyelectrolytes are strongly  
494 charged i.e., remain fully ionized over a wide range of solution  
495 pH. Due to their enhanced stability against hydrolysis,<sup>55</sup>  
496 acrylamido monomers were preferred over acrylates. The  
497 acrylamido group also places hydrophilicity near the backbone,  
498 as opposed to phenyl pendant groups such as those in  
499 poly(styrenesulfonate), a widely used polyelectrolyte.

500 Narrow molecular weight distributions of PMAPTAC and  
501 PAMPS were prepared using classical fractionation techniques

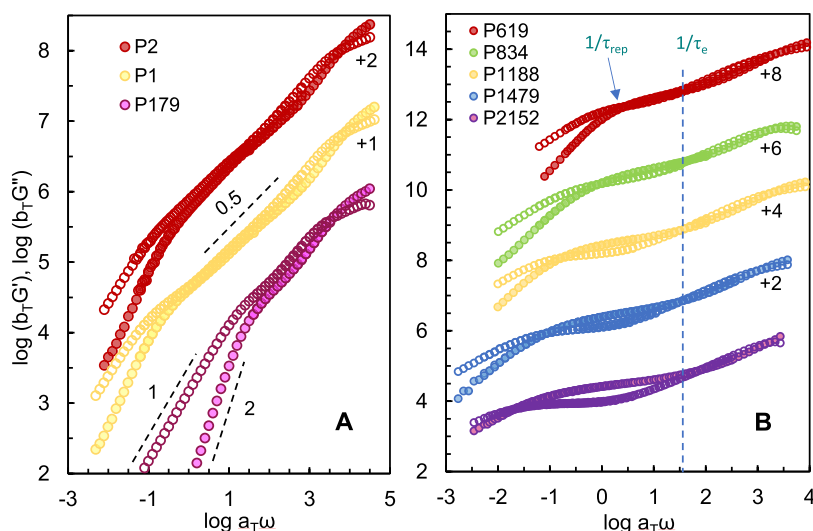


**Figure 6.** Linear viscoelastic response of PMAPTA/PAMPS PECs in 0.01 M NaSCN. Storage and loss modulus,  $G'$  and  $G''$  (Pa), as a function of frequency (in  $\text{rad s}^{-1}$ ). Shift factors  $a_T$  and  $b_T$  for time–temperature superposition are given in Supporting Information Figure S5. Reference temperature is 25 °C. (A) PEC below entanglement and mismatched pairs. (B) Pairs with matched molecular weights, all above the entanglement molecular weight.

**Table 5.** Dynamic Crossover Lifetimes  $\tau_{\text{rep}}$ ,  $\tau_e$ , and  $\tau_0$  (s), Storage Modulus at the Rubbery Plateau  $G_0$  (Pa), Number of Kuhn Segments between Entanglements  $N_e$ , and Zero Shear Viscosity  $\eta_0$  (Pa·s) of the PMAPTA/PAMPS Pairs at  $T_{\text{ref}} = 25$  °C and  $[\text{NaSCN}]_s = 0.01$  M

$P_{\text{nav}}$	$\tau_{\text{rep}}$ (s)	$\tau_e$ (s)	$\tau_0$ (s)	$G_0$ (Pa)	$N_e$	$\eta_0$ (Pa·s)	$G_0 \tau_{\text{rep}}$
P179			$2.5 \times 10^{-4}$			$2.58 \times 10^3$	
P619	0.35	0.029	$3.6 \times 10^{-4}$	38,000	14	$2.35 \times 10^4$	$1.33 \times 10^4$
P834	1.26	0.020	$5.6 \times 10^{-4}$	32,400	16	$5.39 \times 10^4$	$4.08 \times 10^4$
P1188	5.8	0.028	$4.8 \times 10^{-4}$	33,100	16	$1.91 \times 10^5$	$1.89 \times 10^5$
P1479	11.3	0.025	$3.5 \times 10^{-4}$	28,200	19	$2.88 \times 10^5$	$3.19 \times 10^5$
P2152	45.6	0.012	$5.8 \times 10^{-4}$	26,900	20	$1.14 \times 10^6$	$1.23 \times 10^6$
P1			$4.8 \times 10^{-4}$			$2.71 \times 10^3$	
P2			$5.2 \times 10^{-4}$			$2.89 \times 10^3$	

502 (see Table 1 and Figure S1 for details on polyelectrolyte length  
503 and distribution). The polymer chains did not have hydro-  
504 phobic end units, believed to have caused anomalous results in  
505 prior PEC SANS characterization.<sup>56</sup> Solution NMR was used  
506 to verify that PECs were close to stoichiometric (see Table 3  
507 for  $\text{Pol}^+/\text{Pol}^-$  ratios and Figure S2 for NMR spectra and peak  
508 assignments). Nonstoichiometric PECs tend to be softer than  
509 stoichiometric ones because the charge pairing density is lower  
510 and the water content is higher.<sup>57</sup> In the present case, the level  
511 of nonstoichiometry was less than 3%, which was considered  
512 acceptable for the current set of experiments. One well-  
513 entangled polyelectrolyte pair, P1479, was selected for more  
514 intensive studies on the effect of salt content on properties.  
515 Using sensitive radiolabeling techniques, the stoichiometry for  
516 P1479 was determined to be 1.018  $\text{Pol}^+/\text{Pol}^-$  (i.e., 1.8% off-  
517 stoichiometric; Table 2).

518 **Coil Dimensions.** Few studies have been reported on  
519 SANS of synthetic PECs. The first found that chains were close  
520 to Gaussian,<sup>58</sup> a conclusion also reached by Spruijt et al.,<sup>56</sup>  
521 who used PECs made from weak polyelectrolytes poly(acrylic  
522 acid), PAA, and poly(*N,N*-dimethylaminoethyl methacrylate).  
523 However, the estimated Kuhn length in that work varied  
524 strongly from 3.5 to 16 nm. A long Kuhn length would support  
525 the “twisted pair” model of Hamad et al.,<sup>27</sup> but a review by  
526 Larson et al.<sup>29</sup> presents a variety of shorter Kuhn lengths for  
527 charged polymers and concludes the Kuhn high lengths of

Spruijt et al. may be upper limits. Compact Gaussian coils are 528  
529 expected if there are no long-range perturbations, such as  
530 electrostatic repulsions and extensive solvation. All well-paired  
531 PECs are locally neutral and the amount of water admitted to  
532 the PEC is low relative to dilute solution. Fares et al. found  $R_g$   
533 to be independent of salt concentration,<sup>59</sup> in contrast to the  
534 typical response of individual polyelectrolytes, possibly a  
535 consequence of the high  $\text{Pol}^+/\text{Pol}^-$  charge density ( $>1$  M)  
536 within PECs. SANS studies of PECs report a “low  $q$  upturn,”  
537 attributable to density fluctuations approaching the 1  $\mu\text{m}$   
538 length scale, although the materials remain transparent to the  
539 eye.<sup>56,58,60,61</sup> This long-range feature, probably not a result of  
540 thermal fluctuations, as it changes little with temperature  
541 (Figure S4), may be due to weak microphase separation  
542 between deuterated and nondeuterated polymers. The  
543 negligible temperature dependence of coil size in Figure S4  
544 is similar to that found in neutral polymers under  $\theta$ -conditions.  
545 For example, Zirkel et al. found that the  $R_g$  of poly-  
546 (ethylene) in a  $\theta$ -solvent changed by less than 2% over  
547 the same temperature range as that used here.<sup>62</sup>

548 **PEC Stability.** The CSC in NaSCN of three pairs of  
549 PMAPTA/PAMPS was measured using turbidimetry. The  
550 thiocyanate ion is at the hydrophobic end of the Hofmeister  
551 series, making it particularly effective at breaking  $\text{Pol}^+/\text{Pol}^-$   
552 pairs.<sup>63</sup> Low-polydispersity P179, P619, and P1188 yielded  
553 steep room temperature CSCs at around 0.55 M NaSCN

554 (Figure 2). Figure 2 reveals only a mild dependence of CSC on  
 555 molecular weight, as expected for longer polymers. Approaching  
 556 the CSC from low to high  $[\text{NaSCN}]_s$  (the more  
 557 conventional “forwards” method) gives the same result as  
 558 from the reverse method (also known as “desalting”<sup>2,64</sup>). This  
 559 is strong evidence that the composition of this (liquid-like)  
 560 PEC is in equilibrium with the solution composition. Being  
 561 kinetically sluggish, more solid-like PECs are expected to show  
 562 distinct metastable phases.<sup>65</sup>

563 The CSC of wide MWD PMAPTA/PAMPS was found to  
 564 be less sharp (Figure S6) and the forward salt addition did not  
 565 track the desalting curve. Because the effective association  
 566 constant between associated polyelectrolytes in PEC and  
 567 individual polymers in solution is extremely high,<sup>66</sup> over most  
 568  $[\text{MA}]_s < [\text{MA}]_{\text{CSC}}$  negligible amounts of polyelectrolyte are  
 569 expected in the dilute phase, either as individual molecules or  
 570 “quasisoluble” clusters.<sup>67</sup> Quasisoluble PEC nanoparticles are  
 571 favored when there is nonstoichiometry and a length  
 572 mismatch,<sup>68–70</sup> which means for a wide  $\mathcal{D}$  sample, the forward  
 573 addition may not generate the same particle size distributions  
 574 as the reverse, generating hysteresis in the absorbance and  
 575 giving the appearance of metastability.

576 **PEC Ions: Counter- or Co- ?** To date, there are no  
 577 experimental methods that directly indicate whether an ion in a  
 578 PEC is a counterion or a co-ion. Without this knowledge, the  
 579 density of  $\text{Pol}^+\text{Pol}^-$  pairs as a function of  $[\text{salt}]$  remains  
 580 unknown. Presumed fast exchange between the two ion  
 581 environments complicates such a measurement. If the fraction  $f$   
 582 were approximately  $f = 1$ ,  $y = r$ . There are two systems where  $f$  is  
 583 believed to approach 1: glassy PECs have limited free volume,  
 584 forcing  $\text{Pol}^+\text{Pol}^-$  to break at low doping.<sup>23</sup> Alternatively, ions  
 585 with specific affinity for either  $\text{Pol}^+$  or  $\text{Pol}^-$  would bias the  
 586  $\text{MA}_{\text{PEC}}$  population in favor of counterions. Thiocyanate is,  
 587 potentially, such an ion. Affinity (specificity) for  $\text{Pol}^+$  or  $\text{Pol}^-$  is  
 588 revealed by an endothermic heat of complexation: polymer  
 589 pairing causes the loss of a specifically “bound” ion.<sup>51</sup>

590 Isothermal calorimetry (ITC, detailed procedure described  
 591 in the Supporting Information) was carried out to measure the  
 592 heat of complexation,  $\Delta H_{\text{PEC}}$ , between PMAPTA(SCN) and  
 593 PAMPS(Na). The ITC thermogram (Figure S7) showed net  
 594 endothermic complexation with  $\Delta H_{\text{PEC}} = +2255 \text{ J mol}^{-1}$ ,  
 595 indicating significant attractive MA specificity, probably  $\text{SCN}^-$   
 596 for MAPTA<sup>+</sup>. The distribution of MA between PEC and  
 597 supernatant is the result of a Donnan equilibrium, described  
 598 by<sup>51</sup>

$$\frac{[\text{MA}]_{\text{PEC}}}{[\text{MA}]_s} = e^{f\Delta H_{\text{PEC}}/2RT} \quad (10)$$

600 The  $e^{f\Delta H_{\text{PEC}}}$  term represents the departure from an ideal  
 601 Donnan equilibrium driven by entropy alone. If  $f = 1$ , eq 10 for  
 602 the current PEC system would yield  $[\text{NaSCN}]_{\text{PEC}} = 1.58$ –  
 603  $[\text{NaSCN}]_s$ , which is shown as the dotted line, predicting the  
 604 experimental  $[\text{NaSCN}]_{\text{PEC}}$  results in Figure 3 well.

605 A second piece of information supporting the assumption  
 606 that  $f = 1$  over much of the  $[\text{NaSCN}]_{\text{PEC}}$  is obtained by  
 607 extrapolating  $r$  versus  $[\text{NaSCN}]_s$  to  $r = 1$ . At this point, the  
 608 number of salt ions equals the number of polyelectrolyte  
 609 charges and, if  $f = 1$ ,  $y = r$  and the PEC should be dissociated.  
 610 Indeed, at  $r = 1$ , the  $[\text{NaSCN}]_s$  is at the CSC (Figure 3B).

611 As a final and direct indication of the disposition of ions  
 612 within the PEC, FTIR was performed on various  $\text{SCN}^-$ -  
 613 containing systems. The wavelength of the  $\text{C}\equiv\text{N}$  stretch in

614  $\text{SCN}^-$  (and in other cyano systems) is known to depend on  
 615 the solvation environment.<sup>71</sup> This “vibrational solvatochrom-  
 616 ism” can be related to a change in the local electric field, or  
 617 Stark effect, once all of the contributions to this field are  
 618 accounted for. SCN groups are also used as site-specific  
 619 vibrational probes of protein electrostatics.<sup>72</sup> Figure 7 shows a

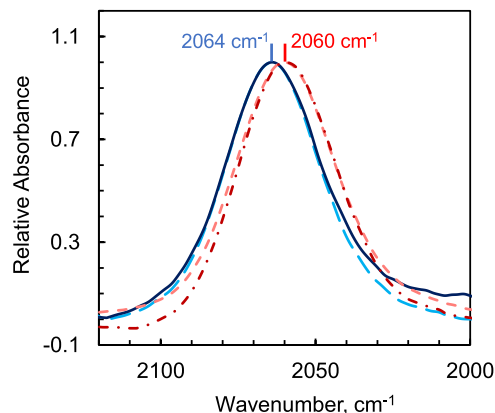


Figure 7. Normalized ATR-FTIR spectra of CN stretch in 1.0 M NaSCN, blue long dash; 0.6 M NaSCN in 1.0 M PAMPS-Na, solid blue line; 1.0 M PAMPTA(SCN), red short-dashed line; and PMAPTA/PAMPS PEC doped in 0.3 M NaSCN, red dash-dot. Spectral resolution,  $0.5 \text{ cm}^{-1}$ . Room temperature. When  $\text{SCN}^-$  is associated with PMAPTA, either in solution or in the PEC, there is a  $\sim 4.6 \text{ cm}^{-1}$  red shift in the  $\text{C}\equiv\text{N}$  absorption band.

620 clear, albeit small,  $4.6 \text{ cm}^{-1}$  shift for  $\text{SCN}^-$  associated with  
 621 PMAPTA<sup>+</sup> in a counterion environment (PMAPTA(SCN)  
 622 solution). The identical shift is seen for  $\text{SCN}^-$  in PEC (in 0.3  
 623 M NaSCN for a doping level of about 0.6), whereas in a  
 624 solution of NaSCN or NaSCN with PAMPS,  $\nu_{\text{SCN}^-}$  is at 2064  
 625  $\text{cm}^{-1}$ , reflecting an unassociated or co-ion environment. This is  
 626 the first reported direct measurement of the ion environment  
 627 within a PEC.  $2060 \text{ cm}^{-1}$  corresponds to a  $6.2 \times 10^{13} \text{ Hz} = 2.6$   
 628  $\times 10^{-15} \text{ s}$  relaxation time, much shorter than the residence time  
 629 of  $\text{SCN}^-$  on MAPTA<sup>+</sup> (about 2 ns at room temp, see below).  
 630 It is assumed that  $\text{SCN}^-$  in a PEC co-ion environment would  
 631 be reflected by intensity at  $2064 \text{ cm}^{-1}$ . All of these pieces of  
 632 evidence support the assumption that  $f = 1$ , at least up to 60%  
 633 doping, and that each NaSCN breaks a charge pair cross-link as  
 634 in Scheme 1. The precise nature of the MAPTA<sup>+</sup>/ $\text{SCN}^-$   
 635 association, whether a contact ion pair or a solvent-separated  
 636 pair, is not known. Though  $\text{SCN}^-$  is more likely to be  
 637 specifically located next to MAPTA<sup>+</sup> than  $\text{Na}^+$  is next to  
 638 AMPS<sup>-</sup>, one  $\text{SCN}^-$  still breaks one  $\text{Pol}^+\text{Pol}^-$  pair.

639 Without a direct measure of  $f$ , and if  $f$  varies as a function of  
 640  $[\text{salt}]$ , it becomes difficult to relate the density of  $\text{Pol}^+\text{Pol}^-$   
 641 pairs to external salt concentration. As long as  $f > 0$ ,  $\text{Pol}^+\text{Pol}^-$   
 642 pairs will be broken on doping and the viscoelasticity will  
 643 change to lower values of moduli and viscosity. Ghasemi et  
 644 al.<sup>24</sup> have computed the value of  $f$  as a function of  $[\text{salt}]$ . If  
 645 there are measurable enthalpy changes on complexation, the  
 646 magnitude of  $f$  may be extracted by determining the ratio  
 647  $[\text{MA}]_{\text{PEC}}/[\text{MA}]_s$  and using eq 10. In certain cases,  $f$  decreases  
 648 with doping, e.g., when  $\Delta H_{\text{PEC}}$  is exothermic, and the product  
 649  $fr$  never reaches 1. In such a scenario, a CSC is not observed.

650 **Nature of the “Sticker”.** Physical interactions between  
 651 polymers are often called “stickers.”<sup>37–39</sup> Charge pairing  
 652 interactions break and reform at a fast rate, about  $5 \times 10^8$   
 653  $\text{s}^{-1}$  at room temperature according to Figure 5. Such a short

654 sticker lifetime is on the order of the fastest relaxation time in  
 655 neutral polymers<sup>3</sup> and would not be effective by itself at  
 656 slowing chain dynamics. In fact, in undoped PECs, there are no  
 657 “available” extrinsic sites, so neighboring two pairs, or a quad of  
 658 charges, must exchange places simultaneously if they are to  
 659 move.<sup>40</sup> Pair exchange has twice the activation energy as pair  
 660 breaking and occurs much more slowly. In effect, almost all of  
 661 the pair breaking events lead to recombination of the same pair  
 662 and only in the rare event that two pairs break simultaneously,  
 663 lifetime  $\tau_q$  can chains move relative to each other. This is an  
 664 example of a “renormalized” sticker lifetime,  $\tau_b^*$ .<sup>37</sup> In the  
 665 present system,  $\tau_q = \tau_b^* = 7.3 \times 10^{-13} \exp\left(\frac{36900}{RT}\right)$  (see Sup-

666 porting Information Figure S8 for more details). To compare  
 667 with the LVR data (Figure 6, Table 5)  $\tau_q$  must be further  
 668 normalized so that  $\tau_0$  represents a Kuhn length of stickers,  
 669 which is 9.4 pairs. The estimated  $\tau_0$  (see the Supporting  
 670 Information) is about  $2 \times 10^{-4}$  s, which is fairly close to the  
 671 value read from the  $\tau_0$  crossover.

672 **Sticky Reptation.** From Figure 6 and Table 5, the  
 673 measured  $G_0$ ,  $\tau_e$ , and  $\tau_0$  do not depend significantly on chain  
 674 length, as expected, whereas  $\tau_{\text{rep}}$  becomes significantly slower  
 675 with longer chains. The terminal region shows the expected  $\omega^1$   
 676 and  $\omega^2$  scaling for  $G''$  and  $G'$ , respectively. The ratio of  $\tau_{\text{rep}}/\tau_e$   
 677 vs  $n_{\text{avg}}$  was used to determine  $n_c$ , the critical number of  
 678 monomer units for entanglement (Figure S9).  $n_c = 347$  ( $N_c =$   
 679 37) was found to be 2–3 times the value of  $n_e$ , which is similar  
 680 to neutral polymers.

681 Below  $n_c$ , only the “monomer time”  $\tau_0$  was observed (Figure  
 682 6A), at values similar to those for entangled pairs. The  
 683 similarity of  $\tau_0$  and viscosity for the mismatched pairs P1 and  
 684 P2 support the assumption that the chain dimensions (i.e.,  
 685 Kuhn lengths) for PMAPTA and PAMPS are similar. In P1  
 686 and P2, the shorter chain is below  $n_c$  and  $G' \approx G'' \sim \omega^{0.5}$ . Over  
 687 much of the frequency range, which are the gel criteria  
 688 according to Winter and Chambon.<sup>73</sup> For these PECs, the  
 689 smaller polyelectrolyte chains act as cross-links between the  
 690 longer chains of opposite charge.

691 The expression for the plateau modulus  $G_0$  depends on  
 692 polymer volume fraction  $\phi$  (for 0.01 M NaSCN  $\phi = 0.45$ ), and  
 693 density,  $\rho$ , and has the form<sup>74</sup>

$$694 \quad G_0 = \frac{4\rho RT\phi}{5M_e} \quad (11)$$

695 where  $M_e$  is the molar mass between entanglements and  $G_0$  is  
 696 assumed to be unaffected by sticker units.<sup>37</sup> The number of  
 697 monomer units between entanglements,  $n_e$ , is  $M_e/M_0$ , where  
 698  $M_0$  is the molar mass of a repeat unit, here an average between  
 699 MAPTA and AMPS of  $196 \text{ g mol}^{-1}$ . Sticky reptation dynamics  
 700 for entangled polymers have been treated theoretically by  
 701 Rubinstein and Semenov<sup>37</sup> and others.<sup>38</sup> The sticky reptation  
 702 time  $\tau_{\text{rep}}$  (also called the “disengagement time”) is<sup>37</sup>

$$703 \quad \tau_{\text{rep}} \approx \tau_b^* (f_s p_{\text{inter}})^2 N / N_e \quad (12)$$

704 where  $f_s$  is the number of stickers per chain,  $\tau_b^*$  is the  
 705 renormalized sticker lifetime, and  $p_{\text{inter}}$  is the fraction of  
 706 intermolecular (as opposed to intramolecular) stickers. In  
 707 PECs, because all polymer repeat units are forced to pair with  
 708 other units,  $p_{\text{inter}} = 1$ . In the LVR data presented in Figure 6  
 709 and Table 5, the relaxation time  $\tau_0$  corresponds to a Kuhn  
 710 length and  $F$  corresponds to the number of Kuhn length  
 711 stickers per chain,  $F = f_s/n_K$ , thus

$$\tau_{\text{rep}} \approx \tau_0 (F)^2 N / N_e \quad (13) \quad 712$$

For undoped PEC,  $F = N$  and 713

$$\tau_{\text{rep}} \approx \tau_0 N^3 / N_e \quad (14) \quad 714$$

$$\eta_0 \approx \frac{\rho RT\phi N^3}{M_e N_e} \tau_0 \approx G_0 \tau_0 \frac{N^3}{N_e} \approx G_0 \tau_{\text{rep}} \quad (15) \quad 715$$

Zero shear viscosities plotted as a function of  $N_{\text{avg}}$  (Figure 8) 716  
 show a scaling of  $\eta_0 \sim N^{3.10}$ , slightly more than the  $N^3$  717

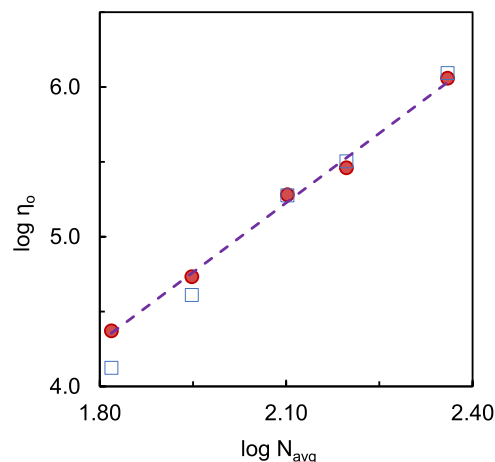


Figure 8. Experimental zero shear viscosity (●, see Figure S10) as a function of chain length for entangled PECs in 0.01 M NaSCN.  $T_{\text{ref}} = 25 \text{ }^\circ\text{C}$ . The measured  $\eta_0$  scales as  $\sim N^{3.10}$  (solid line). Approximate prediction  $\eta_0 \approx G_0\tau_{\text{rep}}$  is shown by the open squares.

718 predicted.<sup>37</sup> A scaling of  $N^{3.4}$  is usually observed for entangled 719  
 polymers.<sup>3</sup> The slightly lower scaling may come from a 720  
 population of unentangled polymers in each fraction.  $\eta_0$ , 721  
 estimated from eq 15, which is an approximation without 722  
 prefactors,<sup>37</sup> is also listed in Table 5 and is in rough agreement 723  
 with experiment. In a previous work using a polycarboxylate,<sup>40</sup> 724  
 a pH-sensitive polyanion, we had obtained a puzzling scaling of 725  
 $\eta_0 \sim N^{5.4}$ , one of the motivations for the present work. It is 726  
 possible that the rapid protonation/deprotonation of the 727  
 carboxylate repeat units provides another channel for 728  
 disengaging  $\text{Pol}^+\text{Pol}^-$  pairs. This might explain why carboxylate 729  
 PECs are usually liquid-like.

730 At sufficiently high temperatures all of the dynamics in a 731  
 polymer chain follow Arrhenius behavior,  $\ln \omega \sim 1/T$ , reflected 732  
 in a linear  $\ln a_T$  versus  $1/T$  plot. Under these conditions, the 733  
 fastest relaxation in the LVR in Figure 6 and Table 5,  $\tau_0$ , 734  
 should be that of a Kuhn length. In the current system, 735  
 Arrhenius response was only observed at temperatures  $>50 \text{ }^\circ\text{C}$  736  
 (Figure S8). To correct the response to what it would have 737  
 been if  $\tau_0$  were measured in the Arrhenius region (it would be 738  
 faster) the measured value of  $\tau_0$  is corrected by the factor 739  
 shown on the graph in Figure S8, which is a factor of about 740  
 0.71. An average  $\tau_0$  of  $4.7 \times 10^{-4}$  s was read from Figure 6 741  
 which yields a corrected  $\tau_0$  of  $3.3 \times 10^{-4}$  s. This is orders of 742  
 magnitude slower than the Kuhn length relaxation time in 743  
 neutral melts and explains the high viscosity of liquid-like 744  
 coacervates, even though the polymer volume fraction is 745  
 decreased significantly by the presence of water.

746 **Breaking Charge Pairs via Doping.** The experimental 747  
 variables in the LVR of PECs are often interrelated by attempts 748

748 at superposition,<sup>29</sup> such as TTS discussed previously. LVR at  
749 various  $[\text{NaSCN}]_s$  was shifted to produce the master curve  
750 shown in Figure 9. The influence of salt was originally<sup>75</sup>

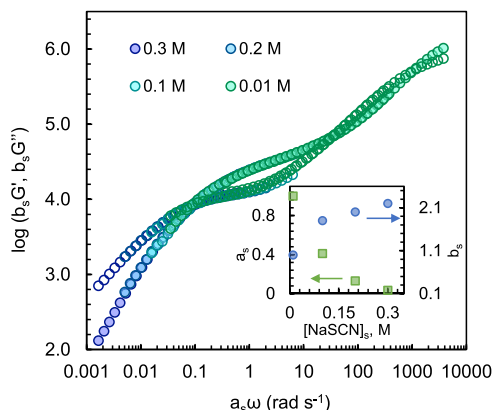


**Figure 9.** Time-salt superposition of P1479 doped with 0.01, 0.1, 0.2, and 0.3 M NaSCN at  $T = 25\text{ }^\circ\text{C}$ . The reference salt concentration is 0.01 M. The inset shows salt shift factors  $a_s$  and  $b_s$ . See Supporting Information Figure S11 for individual time-temperature superposition data.

751 attributed to the control of the lifetime of  $\text{Pol}^+\text{Pol}^-$  interactions  
752 by electrostatic screening. The pair lifetime,  $\tau_{\text{pair}}$  was proposed  
753 to scale with  $[\text{NaCl}]^{0.5}$  as follows:<sup>17</sup>

$$754 \quad \ln \tau_{\text{pair}} \sim A\sqrt{[\text{salt}]} + B \quad (16)$$

755 where  $A$  and  $B$  are constants. Figure 5 shows this lifetime  
756 changes very little with added NaSCN. Eq 16 assumes the  
757 Debye-Hückel approximation to describe electrostatic shield-  
758 ing, in spite of the fact that PECs already contain  $>1$  M charges  
759 from the polyelectrolyte units themselves. Also, the authors  
760 assumed  $\phi$  did not change with  $[\text{salt}]$ . A viscoelasticity study of  
761 a more glassy PEC also employed eq 16 and found an  
762 appropriate salt scaling if  $\phi$  was assumed to decrease with  
763 increasing salt concentration.<sup>30</sup> However, in another study on  
764 length-matched polypeptides, Marciel et al.<sup>36</sup> were unable to  
765 find the scaling of eq 16, and instead found the dynamics  
766 (reported by the shift factor  $a_s$ ) to vary as  $e^{-[\text{NaCl}]}$ , similar to  
767 the response observed here.

768 Attempts at time-salt superposition often produce imper-  
769 fectly overlapping data sets,<sup>29</sup> as seen in Figure 9 in the 1–10  
770  $\text{rad s}^{-1}$  frequency range (see also Figure 9 in ref 25, Figure 4 in  
771 ref 7, and Figure 8 in ref 40). This is because there are at least  
772 three variables—change in polymer volume fraction from  
773 swelling (which changes  $G_0$  and  $N_e$ ), lifetime of  $\text{Pol}^+\text{Pol}^-$  pairs,  
774 and number density of pairs—that are not sufficiently captured  
775 by two shift factors. In contrast to eq 16, the pair lifetime  
776 changes very little over the entire  $[\text{salt}]$  range (see Figure 5B).  
777 The viscosity was measured as a function of  $[\text{NaSCN}]_s$ . At  
778 higher  $[\text{MA}]$ , up to the CSC, the ions continue to exclusively  
779 break  $\text{Pol}^+\text{Pol}^-$ , decreasing the pair density in the complex.  
780 This is paralleled by a decrease in PEC viscosity. Figure 10  
781 gives the zero shear viscosity measured in P1479 as a function  
782 of  $y$ . Figure 10 reveals a leveling of viscosity at the lowest  
783 values of  $y$ , believed to be a consequence of small  
784 nonstoichiometry thus residual ions. The change in viscosity  
785 with salt concentration less pronounced than that observed in  
786 PDADMA/PSS,<sup>34,30,76</sup> a PEC with a glass transition temper-  
787 ature of  $34\text{ }^\circ\text{C}$ , because added salt also decreases  $T_g$ .<sup>25</sup>

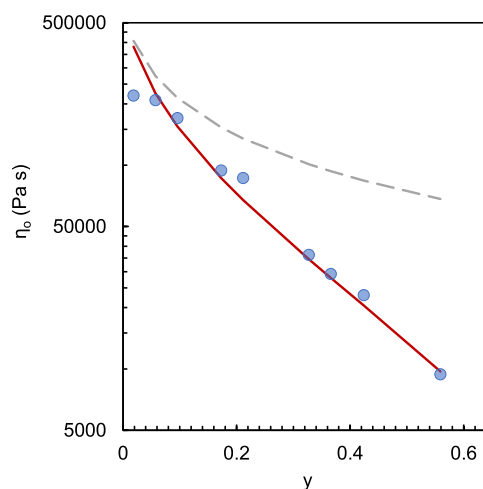


**Figure 10.** Zero shear viscosity of P1479 as a function of  $y$  (from Figure 3B) the fraction of  $\text{Pol}^+\text{Pol}^-$  pairs broken, at  $T_{\text{ref}} = 25\text{ }^\circ\text{C}$ . Viscosities were measured at  $T = 55\text{ }^\circ\text{C}$  (see Supporting Information Figure S10B) and shifted to  $25\text{ }^\circ\text{C}$  using a shift factor  $a_T = 1/0.17$ . The solid line is eq 17 with an intercept fit of  $5 \times 10^5$  Pa·s. The dashed line shows the contribution to  $\eta_0$  from the decreasing polymer volume fraction  $\phi$  only.

The number of Kuhn length stickers  $F$  in eq 13 is now  $(1 - y)N$ . In a  $\theta$ -solvent for entangled polymers,  $\eta_0 \sim \phi^{4.7}$ ,<sup>3</sup> thus the estimated viscosity of the doped PEC,  $\eta_{0,d}$ , relative to undoped,  $\eta_{0,u}$  is

$$792 \quad \eta_{0,d} = \eta_{0,u} \frac{\tau_{0,d}}{\tau_{0,u}} \left( \frac{\phi_d}{\phi_u} \right)^{4.7} (1 - y)^2 \quad (17)$$

The volume fractions come from Table S2, the ratio  $\tau_{0,d}/\tau_{0,u}$  793 for undoped and doped PEC from Figure 5B, and  $y$  is taken 794 from Figure 3B ( $y = r = 1.93[\text{NaSCN}]_s - 0.02$ ). Because the 795 viscosity remains constant at low  $y$ , about  $2.2 \times 10^5$  Pa·s, a fit 796 value of  $5 \times 10^5$  Pa·s was used as  $\eta_{0,u}$  for completely undoped 797 PEC. Eq 17 provides a reasonable fit to most of the data. The 798 decrease in viscosity on doping comes largely from the loss of 799  $\text{Pol}^+\text{Pol}^-$  pairs. The dotted line shows the contribution from 800 the decrease in volume fraction  $\left( \frac{\phi_d}{\phi_u} \right)^{4.7}$ . The  $\eta_0$  at low  $y$  801 coincides with a significant change in  $\phi$  over this region, which 802 is unexpected. Though the cause is presently uncertain, this 803 swelling is thought to be due to residual ions and the osmotic 804 pressure of the PEC matrix. 805

## 806 CONCLUSIONS

A decade of studies in the field have pointed to unique aspects 807 of dynamics within PECs, but full picture of how dynamics at 808 the monomer scale translate to bulk viscoelastic response in 809 PECs has been slow to emerge. The current work has 810 systematically isolated, controlled, and measured the variables 811 needed to provide a quantitative understanding of dynamics in 812 a liquid-like polyelectrolyte coacervate. The dynamics of PECs 813 close to, or below,  $T_g$  will be additionally slowed by 814 cooperativity known to operate in glassy systems approaching 815  $T_g$ . 816

Although individual  $\text{Pol}^+\text{Pol}^-$  dynamics are fast, sticky 817 interactions for undoped PECs act pairwise, via a pair 818 exchange mechanism, responsible for slowing chain motion 819 by orders of magnitude compared to neutral polymers. A Kuhn 820

length “monomer” relaxation time of about 0.3 ms at 25 °C was measured. The dynamics of any PEC will depend critically on  $\tau_0$  and its temperature response. Variations in these parameters probably account for the wide variation of LVR observed for different combinations of  $\text{Pol}^+$  and  $\text{Pol}^-$ .

The use of thiocyanate ion in salt doping has enabled a breakthrough in identifying how many  $\text{Pol}^+\text{Pol}^-$  pairs are broken.  $\text{SCN}^-$  specifically interacts with positive polymer repeat units, ensuring that one added salt breaks one  $\text{Pol}^+\text{Pol}^-$  pair in a site-specific PEC doping model. This specific association of a counterion within a PEC was directly demonstrated, for the first time, using the position of the CN stretching band in FTIR. The viscosity of undoped PECs scaled with  $N^{3.1}$  in line with the sticky reptation model. A relationship for the viscosity of doped PEC was tested using NaSCN as a doping salt. Most of the decrease in viscosity on doping stems from the loss of sticky interactions and not from a modification of the  $\text{Pol}^+\text{Pol}^-$  pair lifetime, as originally proposed.

While every effort was made here to eliminate variables such as the pH-dependence of charge, supplemental H-bonding, polydispersity, mixed functionality, charges separated by neutral units, hydrophobic effects, and nonlinear architecture, some or all of these variables are present in most coacervating systems, especially biological ones. The formation and properties of PECs made from more complex systems remain of great interest.

## ASSOCIATED CONTENT

### Supporting Information

The Supporting Information is available free of charge at <https://pubs.acs.org/doi/10.1021/acs.macromol.3c01540>.

Procedure for radiolabeling ions in PECs; procedure and size exclusion chromatography of polyelectrolytes; isothermal calorimetry method; synthesis of deuterated monomers and polymers;  $^1\text{H}$  NMR spectra of polyelectrolytes and PEC; SANS of PEC at different temperatures; critical salt concentration of wide molecular weight distribution PEC; isothermal calorimetry of PMAPTA(SCN) and PAMPS; compositions of PECs at various  $[\text{NaSCN}]_0$ ; time–temperature superposition of PEC pairs; shift factors for TTS; Arrhenius plot of shift factors; estimation of the critical number of repeat units for entanglement; viscosity of PEC at low shear rates; TTS for PEC in various  $[\text{NaSCN}]_0$ ; and TTS of complex viscosity of PEC pairs (PDF)

## AUTHOR INFORMATION

### Corresponding Author

Joseph B. Schlenoff – Department of Chemistry and Biochemistry, The Florida State University, Tallahassee, Florida 32306, United States; [orcid.org/0000-0001-5588-1253](https://orcid.org/0000-0001-5588-1253); Email: [jshlenoff@fsu.edu](mailto:jshlenoff@fsu.edu)

### Authors

Khalil Akkaoui – Department of Chemistry and Biochemistry, The Florida State University, Tallahassee, Florida 32306, United States

Zachary A. Digby – Department of Chemistry and Biochemistry, The Florida State University, Tallahassee, Florida 32306, United States; [orcid.org/0000-0001-5018-9620](https://orcid.org/0000-0001-5018-9620)

Changwoo Do – Neutron Scattering Division, Oak Ridge National Laboratory, Oak Ridge, Tennessee 37831, United States; [orcid.org/0000-0001-8358-8417](https://orcid.org/0000-0001-8358-8417)

Complete contact information is available at: <https://pubs.acs.org/10.1021/acs.macromol.3c01540>

## Notes

The authors declare no competing financial interest.

## ACKNOWLEDGMENTS

This research used resources at the Spallation Neutron Source, a DOE Office of Science User Facility operated by the Oak Ridge National Laboratory. This research was supported in part by the National Science Foundation, Grant DMR 2103703.

## REFERENCES

- (1) Chen, Y.; Yang, M.; Schlenoff, J. B. Glass Transitions in Hydrated Polyelectrolyte Complexes. *Macromolecules* **2021**, *54*, 3822–3831.
- (2) Bungenberg de Jong, H. G.; Kruyt, H. R. Coacervation (Partial Miscibility in Colloid Systems). *Proc. Sect. Sci. K. Ned. Akad. Wetenschappen* **1929**, *32*, 849–856.
- (3) Rubinstein, M.; Colby, R. H. *Polymer Physics*; Oxford University Press: New York, 2003.
- (4) Rosales, A. M.; Anseth, K. S. The Design of Reversible Hydrogels to Capture Extracellular Matrix Dynamics. *Nat. Rev. Mater.* **2016**, *1*, No. 15012.
- (5) Winne, J. M.; Leibler, L.; Du Prez, F. E. Dynamic Covalent Chemistry in Polymer Networks: A Mechanistic Perspective. *Polym. Chem.* **2019**, *10*, 6091–6108.
- (6) Voorhaar, L.; Hoogenboom, R. Supramolecular Polymer Networks: Hydrogels and Bulk Materials. *Chem. Soc. Rev.* **2016**, *45*, 4013–4031.
- (7) Schaaf, P.; Schlenoff, J. B. Saloplastics: Processing Compact Polyelectrolyte Complexes. *Adv. Mater.* **2015**, *27*, 2420–2432.
- (8) Shamoun, R. F.; Reisch, A.; Schlenoff, J. B. Extruded Saloplastic Polyelectrolyte Complexes. *Adv. Funct. Mater.* **2012**, *22*, 1923–1931.
- (9) Kelly, K. D.; Schlenoff, J. B. Spin-Coated Polyelectrolyte Coacervate Films. *ACS Appl. Mater. Interfaces* **2015**, *7*, 13980–13986.
- (10) Haile, M.; Sarwar, O.; Henderson, R.; Smith, R.; Grunlan, J. C. Polyelectrolyte Coacervates Deposited as High Gas Barrier Thin Films. *Macromol. Rapid Commun.* **2017**, *38*, No. 1600594.
- (11) Gai, M.; Li, W.; Frueh, J.; Sukhorukov, G. B. Polylactic Acid Sealed Polyelectrolyte Complex Microcontainers for Controlled Encapsulation and NIR-Laser Based Release of Cargo. *Colloids Surf., B* **2019**, *173*, 521–528.
- (12) Duan, Y.; Wang, C.; Zhao, M.; Vogt, B. D.; Zacharia, N. S. Mechanical Properties of Bulk Graphene Oxide/Poly(Acrylic Acid)/Poly(Ethylenimine) Ternary Polyelectrolyte Complex. *Soft Matter* **2018**, *14*, 4396–4403.
- (13) Meng, X.; Perry, S. L.; Schiffman, J. D. Complex Coacervation: Chemically Stable Fibers Electrospun from Aqueous Polyelectrolyte Solutions. *ACS Macro Lett.* **2017**, *6*, 505–511.
- (14) Katchalsky, A.; Künzle, O.; Kuhn, W. Behavior of Polyvalent Polymeric Ions in Solution. *J. Polym. Sci.* **1950**, *5*, 283–300.
- (15) Muthukumar, M. 50th Anniversary Perspective: A Perspective on Polyelectrolyte Solutions. *Macromolecules* **2017**, *50*, 9528–9560.
- (16) Overbeek, J. T. G.; Voorn, M. J. Phase Separation in Polyelectrolyte Solutions. Theory of Complex Coacervation. *J. Cell. Comp. Physiol.* **1957**, *49*, 7–26.
- (17) Spruijt, E.; Cohen Stuart, M. A.; van der Gucht, J. Linear Viscoelasticity of Polyelectrolyte Complex Coacervates. *Macromolecules* **2013**, *46*, 1633–1641.
- (18) Schindler, T.; Nordmeier, E. The Stability of Polyelectrolyte Complexes of Calf-Thymus DNA and Synthetic Polycations: 942

- 943 Theoretical and Experimental Investigations. *Macromol. Chem. Phys.*  
944 **1997**, *198*, 1943–1972.
- 945 (19) Schlenoff, J. B. Site-Specific Perspective on Interactions in  
946 Polyelectrolyte Complexes: Toward Quantitative Understanding. *J.*  
947 *Chem. Phys.* **2018**, *149*, No. 163314.
- 948 (20) Ghasemi, M.; Larson, R. G. Future Directions in  
949 Physicochemical Modeling of the Thermodynamics of Polyelectrolyte  
950 Coacervates. *AIChE J.* **2022**, *68*, No. e17646.
- 951 (21) Radhakrishna, M.; Basu, K.; Liu, Y.; Shamsi, R.; Perry, S. L.;  
952 Sing, C. E. Molecular Connectivity and Correlation Effects on  
953 Polymer Coacervation. *Macromolecules* **2017**, *50*, 3030–3037.
- 954 (22) Rumyantsev, A. M.; Johner, A.; Tirrell, M. V.; de Pablo, J. J.  
955 Unifying Weak and Strong Charge Correlations within the Random  
956 Phase Approximation: Polyampholytes of Various Sequences. *Macro-*  
957 *molecules* **2022**, *55*, 6260–6274.
- 958 (23) Yang, M.; Digby, Z. A.; Schlenoff, J. B. Precision Doping of  
959 Polyelectrolyte Complexes: Insight on the Role of Ions. *Macro-*  
960 *molecules* **2020**, *53*, 5465–5474.
- 961 (24) Ghasemi, M.; Friedowitz, S.; Larson, R. G. Analysis of  
962 Partitioning of Salt through Doping of Polyelectrolyte Complex  
963 Coacervates. *Macromolecules* **2020**, *53*, 6928–6945.
- 964 (25) Shamoun, R. F.; Hariri, H. H.; Ghostine, R. A.; Schlenoff, J. B.  
965 Thermal Transformations in Extruded Saloplastic Polyelectrolyte  
966 Complexes. *Macromolecules* **2012**, *45*, 9759–9767.
- 967 (26) Liu, Y. L.; Winter, H. H.; Perry, S. L. Linear Viscoelasticity of  
968 Complex Coacervates. *Adv. Colloid Interface Sci.* **2017**, *239*, 46–60.
- 969 (27) Hamad, F. G.; Chen, Q.; Colby, R. H. Linear Viscoelasticity  
970 and Swelling of Polyelectrolyte Complex Coacervates. *Macromolecules*  
971 **2018**, *51*, 5547–5555.
- 972 (28) Huang, J.; Morin, F. J.; Laaser, J. E. Charge-Density-Dominated  
973 Phase Behavior and Viscoelasticity of Polyelectrolyte Complex  
974 Coacervates. *Macromolecules* **2019**, *52*, 4957–4967.
- 975 (29) Larson, R. G.; Liu, Y.; Li, H. Linear Viscoelasticity and Time-  
976 Temperature-Salt and Other Superpositions in Polyelectrolyte  
977 Coacervates. *J. Rheol.* **2021**, *65*, 77–102.
- 978 (30) Ali, S.; Prabhu, V. Relaxation Behavior by Time-Salt and Time-  
979 Temperature Superpositions of Polyelectrolyte Complexes from  
980 Coacervate to Precipitate. *Gels* **2018**, *4*, 11.
- 981 (31) Yang, M.; Shi, J.; Schlenoff, J. B. Control of Dynamics in  
982 Polyelectrolyte Complexes by Temperature and Salt. *Macromolecules*  
983 **2019**, *52*, 1930–1941.
- 984 (32) Spruijt, E.; Westphal, A. H.; Borst, J. W.; Cohen Stuart, M. A.;  
985 van der Gucht, J. Binodal Compositions of Polyelectrolyte  
986 Complexes. *Macromolecules* **2010**, *43*, 6476–6484.
- 987 (33) Li, L.; Srivastava, S.; Andreev, M.; Marciel, A. B.; de Pablo, J. J.;  
988 Tirrell, M. V. Phase Behavior and Salt Partitioning in Polyelectrolyte  
989 Complex Coacervates. *Macromolecules* **2018**, *51*, 2988–2995.
- 990 (34) Wang, Q. F.; Schlenoff, J. B. The Polyelectrolyte Complex/  
991 coacervate Continuum. *Macromolecules* **2014**, *47*, 3108–3116.
- 992 (35) Syed, V. M. S.; Srivastava, S. Time–Ionic Strength Super-  
993 position: A Unified Description of Chain Relaxation Dynamics in  
994 Polyelectrolyte Complexes. *ACS Macro Lett.* **2020**, *9*, 1067–1073.
- 995 (36) Marciel, A. B.; Srivastava, S.; Tirrell, M. V. Structure and  
996 Rheology of Polyelectrolyte Complex Coacervates. *Soft Matter* **2018**,  
997 *14*, 2454–2464.
- 998 (37) Rubinstein, M.; Semenov, A. N. Dynamics of Entangled  
999 Solutions of Associating Polymers. *Macromolecules* **2001**, *34*, 1058–  
1000 1068.
- 1001 (38) Zhang, Z.; Chen, Q.; Colby, R. H. Dynamics of Associative  
1002 Polymers. *Soft Matter* **2018**, *14*, 2961–2977.
- 1003 (39) Leibler, L.; Rubinstein, M.; Colby, R. H. Dynamics of  
1004 Reversible Networks. *Macromolecules* **1991**, *24*, 4701–4707.
- 1005 (40) Akkaoui, K.; Yang, M.; Digby, Z. A.; Schlenoff, J. B.  
1006 Ultraviscosity in Entangled Polyelectrolyte Complexes and Coac-  
1007 ervates. *Macromolecules* **2020**, *53*, 4234–4246.
- 1008 (41) Digby, Z. A.; Yang, M.; Lteif, S.; Schlenoff, J. B. Salt Resistance  
1009 as a Measure of the Strength of Polyelectrolyte Complexation.  
1010 *Macromolecules* **2022**, *55*, 978–988.
- (42) Tsuchida, E.; Osada, Y.; Abe, K. Formation of Polyion  
Complexes between Polycarboxylic Acids and Polycations Carrying  
Charges in the Chain Backbone. *Makromol. Chem.* **1974**, *175*, 583–  
592.
- (43) Salehi, A.; Larson, R. G. A Molecular Thermodynamic Model  
of Complexation in Mixtures of Oppositely Charged Polyelectrolytes  
with Explicit Account of Charge Association/Dissociation. *Macro-*  
*molecules* **2016**, *49*, 9706–9719.
- (44) Fisher, R. S.; Elbaum-Garfinkle, S. Tunable Multiphase  
Dynamics of Arginine and Lysine Liquid Condensates. *Nat. Commun.*  
**2020**, *11*, No. 4628.
- (45) Digby, Z. A.; Chen, Y.; Akkaoui, K.; Schlenoff, J. B. Bulk  
Biopolyelectrolyte Complexes from Homopolypeptides: Solid “Salt  
Bridges. *Biomacromolecules* **2023**, *24*, 1453–1462.
- (46) Perry, S. L.; Leon, L.; Hoffmann, K. Q.; Kade, M. J.; Priftis, D.;  
Black, K. A.; Wong, D.; Klein, R. A.; Pierce, C. F.; Margossian, K. O.;  
Whitmer, J. K.; Qin, J.; de Pablo, J. J.; Tirrell, M. Chirality-Selected  
Phase Behaviour in Ionic Polypeptide Complexes. *Nat. Commun.*  
**2015**, *6*, No. 6052.
- (47) Gummel, J.; Cousin, F.; Boué, F. Structure Transition in PSS/  
Lysozyme Complexes: A Chain-Conformation-Driven Process, as  
Directly Seen by Small Angle Neutron Scattering. *Macromolecules*  
**2008**, *41*, 2898–2907.
- (48) Fisher, L. W.; Sochor, A. R.; Tan, J. S. Chain Characteristics of  
Poly(2-Acrylamido-2-Methylpropanesulfonate) Polymers. 2. Compar-  
ison of Unperturbed Dimensions and Persistence Lengths. *Macro-*  
*molecules* **1977**, *10*, 955–959.
- (49) Trinh, C. K.; Schnabel, W. Ionic-Strength Dependence of the  
Stability of Polyelectrolyte Complexes - Its Importance for the  
Isolation of Multiply-Charged Polymers. *Angew. Makromol. Chem.*  
**1993**, *212*, 167–179.
- (50) Bungenberg de Jong, H. G.; Kruyt, H. R. *Colloid Science*;  
Elsevier: Amsterdam, 1949; Vol. 2.
- (51) Schlenoff, J. B.; Yang, M.; Digby, Z. A.; Wang, Q. Ion Content  
of Polyelectrolyte Complex Coacervates and the Donnan Equilibrium.  
*Macromolecules* **2019**, *52*, 9149–9159.
- (52) Mongcopa, K. I. S.; Tyagi, M.; Mailoa, J. P.; Samsonidze, G.;  
Kozinsky, B.; Mullin, S. A.; Gribble, D. A.; Watanabe, H.; Balsara, N.  
P. Relationship between Segmental Dynamics Measured by Quasi-  
Elastic Neutron Scattering and Conductivity in Polymer Electrolytes.  
*ACS Macro Lett.* **2018**, *7*, 504–508.
- (53) Crank, J. *The Mathematics of Diffusion*; Clarendon Press:  
Oxford, 1975.
- (54) Helfferich, F. G. *Ion Exchange*; McGraw-Hill: New York, 1962;  
p 624.
- (55) Schönemann, E.; Laschewsky, A.; Rosenhahn, A. Exploring the  
Long-Term Hydrolytic Behavior of Zwitterionic Polymethacrylates  
and Polymethacrylamides. *Polymers* **2018**, *10*, 639.
- (56) Spruijt, E.; Leermakers, F. A. M.; Fokkink, R.; Schweins, R.; van  
Well, A. A.; Cohen Stuart, M. A.; van der Gucht, J. Structure and  
Dynamics of Polyelectrolyte Complex Coacervates Studied by  
Scattering of Neutrons, X-Rays, and Light. *Macromolecules* **2013**, *46*,  
4596–4605.
- (57) Chen, Y.; Yang, M.; Shaheen, S. A.; Schlenoff, J. B. Influence of  
Nonstoichiometry on the Viscoelastic Properties of a Polyelectrolyte  
Complex. *Macromolecules* **2021**, *54*, 7890–7899.
- (58) Markarian, M. Z.; Hariri, H. H.; Reisch, A.; Urban, V. S.;  
Schlenoff, J. B. A Small-Angle Neutron Scattering Study of the  
Equilibrium Conformation of Polyelectrolytes in Stoichiometric  
Saloplastic Polyelectrolyte Complexes. *Macromolecules* **2012**, *45*,  
1016–1024.
- (59) Fares, H. M.; Ghousoub, Y. E.; Delgado, J. D.; Fu, J.; Urban,  
V. S.; Schlenoff, J. B. Scattering Neutrons Along the Polyelectrolyte  
Complex/Coacervate Continuum. *Macromolecules* **2018**, *51*, 4945–  
4955.
- (60) Kuzminskaia, O.; Riemer, S.; Dalglish, R.; Almásy, L.;  
Hoffmann, I.; Gradzielski, M. Structure and Phase Behavior of  
Interpolyelectrolyte Complexes of PDADMAC and Hydrophobically

- 1079 Modified PAA (HM-PAA). *Macromol. Chem. Phys.* **2023**, *224*,  
1080 No. 2200276.
- 1081 (61) Liu, X.; Chapel, J.-P.; Schatz, C. Structure, Thermodynamic  
1082 and Kinetic Signatures of a Synthetic Polyelectrolyte Coacervating  
1083 System. *Adv. Colloid Interface Sci.* **2017**, *239*, 178–186.
- 1084 (62) Zirkel, A.; Richter, D.; Fetters, L. J.; Schneider, D.; Graciano,  
1085 V.; Hadjichristidis, N. A SANS-Based Evaluation of the Chain  
1086 Dimension Temperature Dependence of Poly(Ethylethylene) Under  
1087 Theta-Conditions. *Macromolecules* **1995**, *28*, 5262–5266.
- 1088 (63) Ghostine, R. A.; Shamoun, R. F.; Schlenoff, J. B. Doping and  
1089 Diffusion in an Extruded Saloplastic Polyelectrolyte Complex.  
1090 *Macromolecules* **2013**, *46*, 4089–4094.
- 1091 (64) Mehan, S.; Herrmann, L.; Chapel, J.-P.; Jestin, J.; Berret, J.-F.;  
1092 Cousin, F. The Desalting/Salting Pathway: A Route to Form  
1093 Metastable Aggregates with Tuneable Morphologies and Lifetimes.  
1094 *Soft Matter* **2021**, *17*, 8496–8505.
- 1095 (65) Ma, Y.; Ali, S.; Prabhu, V. M. Enhanced Concentration  
1096 Fluctuations in Model Polyelectrolyte Coacervate Mixtures Along a  
1097 Salt Isopleth Phase Diagram. *Macromolecules* **2021**, *54*, 11338–11350.
- 1098 (66) Lounis, F. M.; Chamieh, J.; Leclercq, L.; Gonzalez, P.; Geneste,  
1099 A.; Prelot, B.; Cottet, H. Interactions between Oppositely Charged  
1100 Polyelectrolytes by Isothermal Titration Calorimetry: Effect of Ionic  
1101 Strength and Charge Density. *J. Phys. Chem. B* **2017**, *121*, 2684–2694.
- 1102 (67) Zhang, P.; Wang, Z.-G. Supernatant Phase in Polyelectrolyte  
1103 Complex Coacervation: Cluster Formation, Binodal, and Nucleation.  
1104 *Macromolecules* **2022**, *55*, 3910–3923.
- 1105 (68) Kabanov, V. M.; Zezin, A. B. Soluble Interpolymeric Complexes  
1106 as a New Class of Synthetic Polyelectrolyte. *Pure Appl. Chem.* **1984**,  
1107 *56*, 343–354.
- 1108 (69) Tsuchida, E.; Osada, Y.; Sanada, K. Interaction of Poly(Styrene  
1109 Sulfonate) with Polycations Carrying Charges in the Chain Backbone.  
1110 *J. Polym. Sci., Part A-1: Polym. Chem.* **1972**, *10*, 3397–3404.
- 1111 (70) Dautzenberg, H.; Radeva, T. Polyelectrolyte Complex  
1112 Formation in Highly Aggregating Systems: Methodical Aspects and  
1113 General Tendencies. In *Physical Chemistry of Polyelectrolytes*,  
1114 *Surfactant Science Series*; Dekker: New York, 2001; Vol. 99, pp  
1115 743–792.
- 1116 (71) Lee, H.; Choi, J.-H.; Cho, M. Vibrational Solvatochromism and  
1117 Electrochromism of Cyanide, Thiocyanate, and Azide Anions in  
1118 Water. *Phys. Chem. Chem. Phys.* **2010**, *12*, 12658–12669.
- 1119 (72) Adhikary, R.; Zimmermann, J.; Dawson, P. E.; Romesberg, F. E.  
1120 Temperature Dependence of CN and SCN IR Absorptions Facilitates  
1121 Their Interpretation and Use as Probes of Proteins. *Anal. Chem.* **2015**,  
1122 *87*, 11561–11567.
- 1123 (73) Winter, H. H. Can the Gel Point of a Cross-Linking Polymer  
1124 Be Detected by the  $G' - G''$  Crossover? *Polym. Eng. Sci.* **1987**, *27*,  
1125 1698–1702.
- 1126 (74) Fetters, L. J.; Lohse, D. J.; Richter, D.; Witten, T. A.; Zirkel, A.  
1127 Connection between Polymer Molecular Weight, Density, Chain  
1128 Dimensions, and Melt Viscoelastic Properties. *Macromolecules* **1994**,  
1129 *27*, 4639–4647.
- 1130 (75) Spruijt, E.; Sprakel, J.; Lemmers, M.; Stuart, M. A. C.; van der  
1131 Gucht, J. Relaxation Dynamics at Different Time Scales in  
1132 Electrostatic Complexes: Time-Salt Superposition. *Phys. Rev. Lett.*  
1133 **2010**, *105*, No. 208301.
- 1134 (76) Liu, Y.; Momani, B.; Winter, H. H.; Perry, S. L. Rheological  
1135 Characterization of Liquid-to-Solid Transitions in Bulk Polyelec-  
1136 trolyte Complexes. *Soft Matter* **2017**, *13*, 7332–7340.